Self-similar vortex configurations: Collapse, expansion, and rigid-vortex motion

Sreethin Sreedharan Kallyadan* and Priyanka Shukla†
Department of Mathematics, Indian Institute of Technology Madras, Chennai 600036, India

(Received 6 June 2022; accepted 2 November 2022; published 28 November 2022)

The problem of finding initial conditions that lead to self-similar motion of point vortices is formulated as a linear system. The linearity in the equations is used to check for the existence of similarity solutions with a given shape and, in particular, to numerically find self-similar vortex configurations with or without any prior knowledge of circulations. Algorithms for computing the one-parameter family of collapse and expansion configurations and the finitely many rigid-vortex configurations present in the family are also discussed. Typical families are shown to have vortices parametrized along closed curves, and the conditions for which they are not closed are investigated via several numerical examples.

DOI: 10.1103/PhysRevFluids.7.114701

I. INTRODUCTION

The point-vortex model [1] is a discrete vortex approximation widely used to describe the motion of mutually interacting coherent vortical structures in a two-dimensional incompressible ideal fluid. In this model, a vortex is identified as a vorticity singularity in an otherwise irrotational flow. Although the complexities associated with the internal vortex structure are ignored, the framework is capable of approximating the solutions of two-dimensional Euler equations [2–6] and tracking the vorticity maximum dependably [7–9]. Furthermore, the equation of motion of N interacting point vortices of circulations Γ_α and coordinate functions (x_α, y_α) on the unbounded plane is in the form of an analytically approachable Hamiltonian system [10]

$$\Gamma_\alpha \frac{dx_\alpha}{dt} = \frac{\partial \mathcal{H}}{\partial y_\alpha} \quad \text{and} \quad \Gamma_\alpha \frac{dy_\alpha}{dt} = -\frac{\partial \mathcal{H}}{\partial x_\alpha}, \tag{1}$$

with the Hamiltonian being

$$\mathcal{H} = -\frac{1}{4\pi} \sum_{\alpha \neq \beta} \Gamma_\alpha \Gamma_\beta \log \sqrt{(x_\alpha - x_\beta)^2 + (y_\alpha - y_\beta)^2}, \tag{2}$$

where $\alpha, \beta = 1, 2, \ldots, N$, and t denotes the time. Investigating the solutions of (1), the N-vortex problems, help us to gain insights into the elementary processes that govern the mixing and transport in turbulent flows [11].

One of the most intriguing phenomena associated with the N-vortex problems is the existence of vortex collapse solutions, i.e., for specific sets of circulations and initial vortex positions, point vortices would coalesce into the constant of the motion known as the center of vorticity $(\sum \Gamma_\alpha x_\alpha, \sum \Gamma_\alpha y_\alpha)/\sum \Gamma_\alpha$ in finite time. After the collapse, there are no solution continuations via point vortices. This particular singular nature of the vortex trajectories is unlike any two-dimensional

*sreethin2@gmail.com
†priyanka@iitm.ac.in

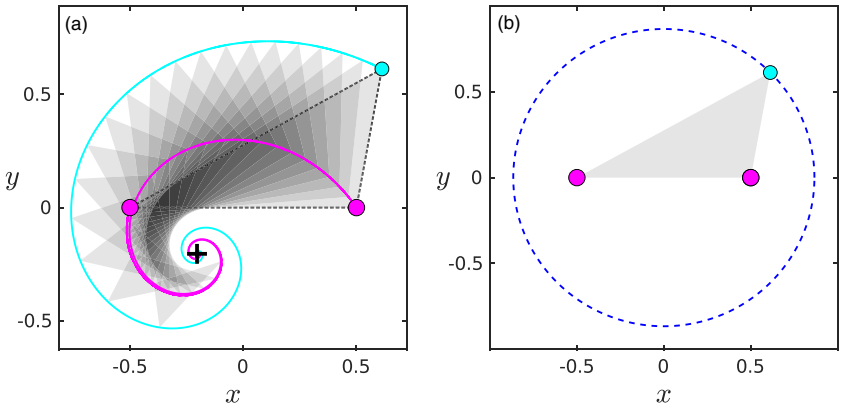

FIG. 1. Example of (a) three-vortex collapse showing the initial vortex positions (filled circles) and the collapse trajectories (solid lines) wherein vortices with circulations $\Gamma_1 = 1 = \Gamma_2$, $\Gamma_3 = -\frac{1}{2}$ move in logarithmic spirals and simultaneously collide at the center of vorticity (+ symbol) in finite time. Vortex triangles at different instances of time are shown as shaded triangles, and they are all similar to the initial vortex triangle (dotted triangle). (b) The family of collapse and expansion initial conditions associated with the circulations $\Gamma_1 = 1 = \Gamma_2$, $\Gamma_3 = -\frac{1}{2}$ given by the parametrization $(x_1, y_1) = (-0.5, 0)$, $(x_2, y_2) = (0.5, 0)$, and $(x_3(\theta), y_3(\theta)) = \sqrt{3}/2\,(\cos\theta, \sin\theta)$, $0 \leqslant \theta < 2\pi$, following the construction from [23,27]. The case $\theta = \pi/4$ (filled circles) corresponds to the collapse initial condition described in Fig. 1(a).

Euler flow, which it is supposed to be approximating and is theorized to be related to the loss of uniqueness of solutions of Euler equations [12]. Moreover, the mechanism of vortex collapse is considered an important elementary act in two-dimensional turbulent kinetics [13–18] since it brings about different length scales to the system. Recently, it was also shown that the collapse of three point vortices results in anomalous enstrophy dissipation [19,20], a characterizing property of two-dimensional turbulence.

The collapse phenomenon in the simplest three-vortex case has been studied extensively in the literature and is well understood [12,15,21–29]. For instance, it is known that the three-vortex collapse is always self-similar [28], i.e., the triangle obtained by joining the location of the three vortices retains the initial triangular shape throughout the motion [see Fig. 1(a)].

While there are counterexamples reported on the sphere [30], all known N-vortex collapses on the unbounded plane stem from such shape-invariant evolution of vortices, hereafter referred to as self-similar collapses. The collection of self-similar collapse initial conditions associated with a circulation set often arise as a one-dimensional continuum wherein the initial vortex positions vary along smooth planar curves [see Fig. 1(b)]. Along such a family of initial conditions, the associated collapse time and Hamiltonian also vary continuously. Aside from the size contraction in self-similar collapse, intervortex distances may also increase or remain constant during a self-similar evolution. They are, respectively, called self-similar expansions and rigid-vortex motions. While the self-similar collapse of three vortices is completely understood, little is known in general about self-similar collapses in larger vortex systems apart from the following two necessary conditions [24] on circulations and intervortex distances:

$$\sum_{\alpha\neq\beta} \Gamma_\alpha \Gamma_\beta = 0, \tag{3a}$$

$$\sum_{\alpha\neq\beta} \Gamma_\alpha \Gamma_\beta \left((x_\alpha - x_\beta)^2 + (y_\alpha - y_\beta)^2\right) = 0. \tag{3b}$$

Although a few self-similar collapse initial conditions of smaller vortex systems are known exactly [12,31,32], gaining meaningful insights into the collapse phenomenon in the larger point-vortex systems necessitates a robust numerical formulation of the problem and that defines the main objective of this work.

For prescribed values of circulations satisfying (3a), several self-similar collapse examples have been constructed in recent times [33,34] by numerically solving for the initial vortex positions from the following algebraic system described by O'Neil [35]:

$$\sum_{\alpha=1}^{N} \Gamma_\alpha (x_\alpha + \mathbb{i} y_\alpha) = 0, \tag{4a}$$

$$\sum_{\alpha=1}^{N} \Gamma_\alpha \left(x_\alpha^2 + y_\alpha^2\right) = 0, \tag{4b}$$

$$v_\alpha \, (x_1 + \mathbb{i} y_1) - v_1 \, (x_\alpha + \mathbb{i} y_\alpha) = 0, \tag{4c}$$

where $\mathbb{i} = \sqrt{-1}$, $2 \leqslant \alpha \leqslant N-2$, and $v_\alpha = dx_\alpha/dt + \mathbb{i}\, dy_\alpha/dt$ is the α^{th} vortex velocity in complex form, functionally expressed in terms of the vortex locations and circulations. Additionally, following the numerical approach, it is also possible to iteratively find the family of self-similar collapse initial conditions by specifying the Hamiltonian, i.e., incorporating the equation

$$\mathcal{H} = \mathcal{H}_0, \tag{5}$$

with the above list of equations (4) and varying the value of $\mathcal{H}_0$ to find different collapse initial conditions of the same circulation set (e.g., see Kudela [34] and Gotoda [36]).

In this work, the problem of finding initial conditions leading to self-similar evolution of point vortices is looked at from scratch by focusing on the ratios of intervortex distances. The resultant algebraic system is a simple $Ax = b$ type matrix system, where A is a matrix in terms of the vortex coordinates, x is the circulations, and b involves a collision time parameter, respectively. The formulation generalizes the existing linear algebra formulation on rigid-vortex configurations studied by Newton and Chamoun [37] and Barreiro *et al.* [38], wherein the constant intervortex distance condition yields an $Ax = 0$ type matrix system. The linearity enables us to search for self-similar collapse configurations without knowing the circulations beforehand. Moreover, concepts from linear algebra, such as singular values and least-square solutions, can be used to numerically quantify how close a generic initial condition is to that of a self-similar one. In contrast to Kudela [34] and Gotoda [36], in this work finding the family of collapse initial conditions is based on a smoothness assumption and does not require perturbing the Hamiltonian or any other parameters.

This paper is organized as follows. A necessary and sufficient condition for the self-similar motion of point vortices is formulated in Sec. II. The formulation is used to describe the distribution of self-similar vortex configurations of three and four vortices in Sec. III. Three error functions, which stem from the formulation and a description of a random walk procedure to minimize them, are given in Sec. IV. The error functions are used appropriately to find and describe several numerical examples of individual self-similar collapse configurations (Sec. V), the family of collapse and expansion configurations (Sec. VI), and rigid-vortex configurations associated with the family (Sec. VII). The findings are summarized in Sec. VIII.

II. PROBLEM FORMULATION AND GOVERNING EQUATIONS

Consider N-point vortices on the unbounded plane, indexed $\alpha = 1, 2, \ldots N$, with $z_\alpha(t) = (x_\alpha(t), y_\alpha(t))$ being the Cartesian coordinate of α^{th} vortex at time t. Evaluating (1), we obtain the

governing equations of vortex motion as

$$\frac{dx_\alpha}{dt} = \frac{-1}{2\pi} \sum_{\beta=1}^{N}{}' \Gamma_\beta \frac{(y_\alpha - y_\beta)}{l_{\alpha\beta}^2}, \tag{6a}$$

$$\frac{dy_\alpha}{dt} = \frac{1}{2\pi} \sum_{\beta=1}^{N}{}' \Gamma_\beta \frac{(x_\alpha - x_\beta)}{l_{\alpha\beta}^2}, \tag{6b}$$

where $l_{\alpha\beta} = \sqrt{(x_\alpha - x_\beta)^2 + (y_\alpha - y_\beta)^2}$ denotes the distance between α and β vortices, and the primed sum is used to indicate that the $\beta = \alpha$ case is excluded from the summation (see Ref. [39] for more details). Note that (6) is undefined in the event of a vortex collision, i.e., at some specific time $t \geqslant 0$, at least one of the intervortex distances satisfies $l_{\alpha\beta} = 0$. In the event of a vortex collision, the point-vortex model (6) fails, and no further analysis is possible. Therefore, we shall assume that the initial vortex coordinates $k_\alpha = z_\alpha(0)$ are such that $k_\alpha \neq k_\beta$ if $\alpha \neq \beta$. For any such initial condition, vortex motion is well defined for $t \in [0, t_c)$, where $t_c > 0$ is the collision time if the initial condition leads to a finite-time vortex collision, and if not, $t_c = \infty$. Using (6), one can derive the following useful expression for the squared intervortex distance derivative (see Chap. 2 of Ref. [39]):

$$\frac{d}{dt}\left(l_{\alpha\beta}^2\right) = \frac{2}{\pi} \sum_{\gamma=1}^{N}{}'' \Gamma_\gamma A_{\alpha\beta\gamma} \left(\frac{1}{l_{\beta\gamma}^2} - \frac{1}{l_{\alpha\gamma}^2} \right), \tag{7}$$

where the double-primed sum is used to indicate that the two cases $\gamma = \alpha$ and β are excluded from the summation, and

$$A_{\alpha\beta\gamma} = \tfrac{1}{2}[(x_\beta - x_\gamma)(y_\beta - y_\alpha) - (x_\beta - x_\alpha)(y_\beta - y_\gamma)] \tag{8}$$

represents the (signed) area of the triangle $\Delta_{\alpha\beta\gamma}$ obtained by joining the three vortex coordinates z_α, z_β, and z_γ in that specific order. The quantity $A_{\alpha\beta\gamma}$ is positive (negative) if $\Delta_{\alpha\beta\gamma}$ is counterclockwise (clockwise).

The system of differential equations (6) together with an initial condition $z_\alpha(0) = k_\alpha$ represents an initial value problem. Since the right-hand side expressions in (6) are smooth functions, the local existence of a unique solution is always guaranteed for any set of distinct initial vortex positions k_α [40]. For $N \geqslant 4$, vortex trajectories generally tend to be chaotic and extremely sensitive to the initial conditions [11].

Given the vortex positions at some time $t \geqslant 0$, we shall refer to the polygonal geometrical object formed by joining the location of the vortices as a *vortex configuration* (see Fig. 2). This work focuses on finding the special solutions of (6), referred to as the similarity solutions (the corresponding physical act of vortex motion referred to as the self-similar motion), for which the shape of the vortex configuration is time invariant. Before we move on to mathematically formulate this concept, let us first discuss the degenerate case when all vortices lie on a straight line (i.e., collinear vortex configurations).

Remark (*Collinear configurations*). The notion of a constant shape, which here is a two-dimensional concept, runs into problems when the N vortices are collinear. Suppose we define a constant "line shape" as vortices retaining collinearity throughout the motion. All vortex triplets must then have zero areas initially and for all time. Thus, it follows from (7) that such a vortex motion, when it exists, must correspond to a collinear rigid-vortex motion and vice versa. They can be found by expressing the following system of equations,

$$A_{\alpha\beta\gamma} = 0 \quad \text{and} \quad \frac{d}{dt}(A_{\alpha\beta\gamma}) = 0, \quad 1 \leqslant \alpha < \beta < \gamma \leqslant N \tag{9}$$

in terms of the intervortex distances and then solving for them from the resulting algebraic system. In this work, we shall assume that the initial vortex positions k_α are noncollinear unless mentioned otherwise. Since the two-vortex case is trivial and all collinear, we shall also assume that $N \geqslant 3$.

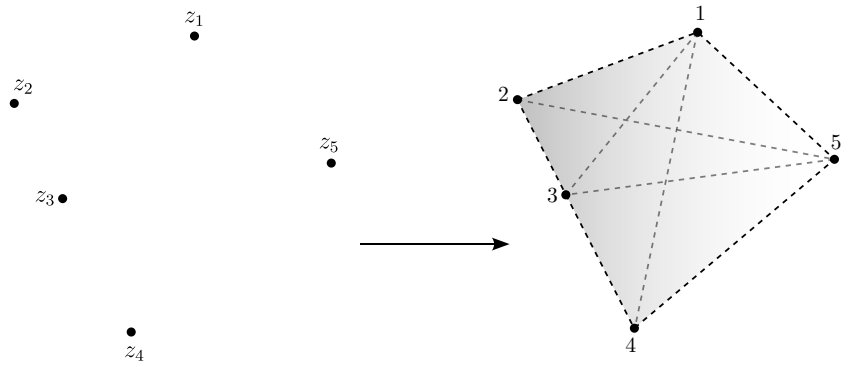

FIG. 2. Schematic showing the relation between vortex coordinates (left) and its associated vortex configuration (right). The overall shape of the configuration is highlighted via shading. It can be seen that a vortex configuration is made up of several vortex triangles and if the angles of all these vortex triangles remain constant during the motion, then the shape of the original configuration also remains constant.

In order for the vortex configuration to have a constant geometrical shape throughout the motion, it is necessary and sufficient that for any three distinct vortices α, β, γ, the angles of the triangle $\Delta_{\alpha\beta\gamma}$ remain constant. Since any angle can be expressed in terms of the ratios of side lengths of the triangle using the cosine rule, it suffices to show that the ratios of all pairs of intervortex distances are constant. As similar triangles must have the side lengths proportional, a constant ratio of intervortex distances is also a necessary condition. Hence, we define a similarity solution as any solution of (6) with the property that

$$\frac{d}{dt}\left[\frac{l_{\alpha\beta}}{l_{\gamma\delta}}\right] = 0, \quad t \in [0, t_c) \tag{10}$$

for all vortex indices $\alpha, \beta, \gamma, \delta$ with $\alpha \neq \beta$ and $\gamma \neq \delta$. Note that it is equivalent to consider the squared ratios $l^2_{\alpha\beta}/l^2_{\gamma\delta}$ in definition (10) instead of the ratios $l_{\alpha\beta}/l_{\gamma\delta}$, as $l_{\alpha\beta}/l_{\gamma\delta}$ is strictly positive in $[0, t_c)$, and therefore

$$\frac{d}{dt}\left[\frac{l^2_{\alpha\beta}}{l^2_{\gamma\delta}}\right] = 2\left(\frac{l_{\alpha\beta}}{l_{\gamma\delta}}\right) \times \frac{d}{dt}\left[\frac{l_{\alpha\beta}}{l_{\gamma\delta}}\right] = 0 \iff \frac{d}{dt}\left[\frac{l_{\alpha\beta}}{l_{\gamma\delta}}\right] = 0. \tag{11}$$

Furthermore, it suffices to fix the denominator indices, say $\gamma = 1$ and $\delta = 2$ in definition (10), and only show that ratios involving l_{12} are constants as it implies any ratio $l_{\alpha\beta}/l_{\gamma\delta} = (l_{\alpha\beta}/l_{12})/(l_{\gamma\delta}/l_{12})$ is also a constant. Therefore, we have the following equivalent definition for the self-similar motion of point vortices.

Definition (Similarity solution). A solution of (6) is said to be a similarity solution if for all indices α, β with $\alpha \neq \beta$

$$\frac{d}{dt}\left[\frac{l^2_{\alpha\beta}}{l^2_{12}}\right] = 0, \quad t \in [0, t_c). \tag{12}$$

The definition (12) indicates that the similarity solutions are nothing but the equilibrium points in the phase plane constituted by the squared ratios of intervortex distances of the form $l^2_{\alpha\beta}/l^2_{12}$. Therefore, we look for the equilibrium points of the following nonautonomous first-order dynamical system

$$\frac{d}{dt}\left[\frac{l^2_{\alpha\beta}}{l^2_{12}}\right] = \frac{1}{l^4_{12}}\left(l^2_{12}\frac{d}{dt}\left(l^2_{\alpha\beta}\right) - l^2_{\alpha\beta}\frac{d}{dt}\left(l^2_{12}\right)\right), \quad 1 \leqslant \alpha < \beta \leqslant N. \tag{13}$$

The equilibrium points of (13) are the solutions of the following system of algebraic equations wherein the derivatives have functional expressions as given by (7),

$$l_{12}^2 \frac{d}{dt}\left(l_{\alpha\beta}^2\right) - l_{\alpha\beta}^2 \frac{d}{dt}\left(l_{12}^2\right) = 0, \quad 1 \leqslant \alpha < \beta \leqslant N \tag{14}$$

or, equivalently,

$$\frac{1}{l_{\alpha\beta}^2}\frac{d}{dt}\left(l_{\alpha\beta}^2\right) = \frac{1}{l_{12}^2}\frac{d}{dt}\left(l_{12}^2\right), \quad 1 \leqslant \alpha < \beta \leqslant N. \tag{15}$$

Note that (15) has no explicit time dependency and can be entirely expressed in terms of the vortex coordinates and circulations. Consequently, finding an initial condition for a similarity solution boils down to finding a set of N coordinate-circulation pairs $(k_\alpha, \Gamma_\alpha)$'s, which algebraically solve (15). Suppose the initial vortex coordinates k_α's and circulations Γ_α's satisfy (15). Let $\lambda_0 = \dfrac{1}{l_{12}^2}\dfrac{d}{dt}(l_{12}^2)|_{t=0}$. It follows that

$$\begin{bmatrix} \frac{1}{l_{12}^2}\frac{d}{dt}\left(l_{12}^2\right) \\ \frac{1}{l_{13}^2}\frac{d}{dt}\left(l_{13}^2\right) \\ \vdots \\ \frac{1}{l_{\alpha\beta}^2}\frac{d}{dt}\left(l_{\alpha\beta}^2\right) \\ \vdots \\ \frac{1}{l_{(N-1)N}^2}\frac{d}{dt}\left(l_{(N-1)N}^2\right) \end{bmatrix}_{t=0} = \begin{bmatrix} \lambda_0 \\ \lambda_0 \\ \vdots \\ \lambda_0 \\ \vdots \\ \lambda_0 \end{bmatrix}. \tag{16}$$

Conversely, any set of N coordinate-circulation $(k_\alpha, \Gamma_\alpha)$ pairs, which satisfy (16) for some $\lambda_0 \in \mathbb{R}$, is an initial condition for a self-similar motion as it also solves (15). Expanding each $N(N-1)/2$ left-hand side expression as a linear combination of circulations using (7), we finally end up with a linear system

$$M\Gamma = \Lambda, \tag{17}$$

where $M = M(k_1, k_2, \ldots, k_N)$ is the $N(N-1)/2 \times N$ configuration matrix given solely by the vortex coordinates as

$$M = \frac{2}{\pi}\begin{bmatrix} 0 & 0 & \frac{A_{123}}{l_{12}^2}\left(\frac{1}{l_{23}^2} - \frac{1}{l_{13}^2}\right) & \cdots & \frac{A_{12N}}{l_{12}^2}\left(\frac{1}{l_{2N}^2} - \frac{1}{l_{1N}^2}\right) \\ 0 & \frac{A_{132}}{l_{13}^2}\left(\frac{1}{l_{32}^2} - \frac{1}{l_{12}^2}\right) & 0 & \cdots & \frac{A_{13N}}{l_{13}^2}\left(\frac{1}{l_{3N}^2} - \frac{1}{l_{1N}^2}\right) \\ \vdots & \vdots & \vdots & \ddots & \vdots \\ \frac{A_{(N-1)N1}}{l_{(N-1)N}^2}\left(\frac{1}{l_{N1}^2} - \frac{1}{l_{(N-1)1}^2}\right) & \frac{A_{(N-1)N2}}{l_{(N-1)N}^2}\left(\frac{1}{l_{N2}^2} - \frac{1}{l_{(N-1)2}^2}\right) & \frac{A_{(N-1)N3}}{l_{(N-1)N}^2}\left(\frac{1}{l_{N3}^2} - \frac{1}{l_{(N-1)3}^2}\right) & \cdots & 0 \end{bmatrix},$$

$\Gamma = [\Gamma_1, \Gamma_2, \ldots, \Gamma_N]^\mathsf{T}$ is the circulation as a column vector, and $\Lambda = [\lambda_0, \lambda_0, \ldots, \lambda_0]^\mathsf{T}$ is a column vector of length $N(N-1)/2$ whose entries are all equal. Although represented as a function of initial vortex positions, calculating the configuration matrix does not require the exact initial vortex coordinates; rather, only the geometric knowledge of the vortex configuration associated with the initial condition, i.e., the orientations of the vortex triplets and inter-vortex distances, is sufficient. Since one can find infinitely many coordinate representations for the same vortex configuration, it is preferable to discuss the initial conditions in terms of the vortex configurations than in the initial vortex coordinates. We henceforth refer to vortex configurations satisfying (17) for some $\Gamma \neq 0$ and $\lambda_0 \in \mathbb{R}$ as *self-similar vortex configurations*.

Next, we shall discuss the physical role of the parameter λ_0 in determining the type of self-similar motion that results from an initial condition satisfying (17). Since the signed area function (8)

is continuous, it can not change the sign without the vortex triangle going through a collinear configuration. Hence, in a self-similar motion of vortices, where the angles remain the same throughout, the orientation of individual vortex triplets will be preserved. From (7), observe that the derivative of any squared intervortex distance can be expressed purely in terms of the intervortex distance ratios and the signs of vortex triangle orientations; therefore, in a self-similar motion, these derivatives are constant functions, i.e.,

$$\frac{d}{dt}\left(l_{\alpha\beta}^2\right) = c_{\alpha\beta} \Rightarrow l_{\alpha\beta}^2(t) = l_{\alpha\beta}^2(0) + c_{\alpha\beta}\, t, \tag{18}$$

where $c_{\alpha\beta} = \frac{d}{dt}(l_{\alpha\beta}^2)|_{t=0} \in \mathbb{R}$. Since the motion is assumed to be self-similar, (17) is satisfied for some $\lambda_0 \in \mathbb{R}$ at $t = 0$. Consequently,

$$\frac{c_{\alpha\beta}}{l_{\alpha\beta}^2(0)} = \lambda_0 \Rightarrow l_{\alpha\beta}^2(t) = l_{\alpha\beta}^2(0)(1 + \lambda_0\, t). \tag{19}$$

It follows that, depending on the sign of λ_0, three types of self-similar motions are possible.

(i) Rigid-vortex motion ($\lambda_0 = 0$) has constant intervortex distances, i.e., $l_{\alpha\beta}(t) = l_{\alpha\beta}(0)$ for any $t \geqslant 0$. Consequently, the whole vortex configuration moves like a rigid body. Such a rigid configuration can generally be translating, rotating (relative equilibria), or even stationary (fixed equilibria). Since no vortex collisions are possible, the motion is well defined for $t \in [0, \infty)$. We henceforth refer to self-similar vortex configurations with $\lambda_0 = 0$ as *rigid-vortex configurations*.

(ii) Self-similar expansion ($\lambda_0 > 0$) has the intervortex distances monotonically increasing with time. Hence, during the motion, the vortex configuration expands while keeping the overall shape constant. The vortex motion is well defined for $t \in [0, \infty)$ and $l_{\alpha\beta} \to \infty$ as $t \to \infty$. We henceforth refer to self-similar vortex configurations with $\lambda_0 > 0$ as *self-similar expansion configurations*.

(iii) Self-similar collapse ($\lambda_0 < 0$) has the intervortex distances monotonically decreasing, reaching the zero value simultaneously at time $t_c = -1/\lambda_0$. Therefore, in a self-similar collapse, the vortex configuration shrinks over time, and the vortices collapse to a single point in finite time while keeping the shape constant. Note that the motion of point vortices is well defined only for $t \in [0, t_c)$, unlike the other two cases. We henceforth refer to self-similar vortex configurations with $\lambda_0 < 0$ as *self-similar collapse configurations*.

Thus, λ_0, which was defined as the initial rate of change of $\log(l_{12}^2)$, becomes an important parameter in a self-similar vortex motion as it coincides with the initial rate of change of any other $\log(l_{\alpha\beta}^2)$. The sign of λ_0 determines the type of self-similar motion executed by the point vortices and is directly related to the collision time in a self-similar collapse. Now, we shall discuss some properties and redundancies associated with the solutions of linear system (17).

(a) *Trivial solution:* (17) is trivially satisfied by any N distinct vortex coordinates, if $\Gamma_1 = \Gamma_2 = \cdots = \Gamma_N = 0$ with $\lambda_0 = 0$.

(b) *Degeneracy:* The linear algebra formulation (17) is not a sufficient criterion for self-similar motion in the case of collinear vortex configurations. Since all triangle areas are zero, the configuration matrix M is a zero matrix in this case. Hence, any set of N vortex circulations would satisfy (17) with the associated $\lambda_0 = 0$.

(c) *Timescale:* Let $(k_\alpha, \Gamma_\alpha)$ be a solution to (17) for some $\lambda_0 \in \mathbb{R}$ and let $c \neq 0$ be any nonzero real number. It follows that $(k_\alpha, c\,\Gamma_\alpha)$ is also a solution to (17), with λ_0 getting scaled as $c\lambda_0$. Each such pair corresponds to a different choice of timescale. We shall use this property while constructing the numerical method in Sec. IV A.

(d) *Equivalent configurations:* Let $(k_\alpha, \Gamma_\alpha)$ be a solution to (17) for some $\lambda_0 \in \mathbb{R}$. We shall call a configuration k'_α to be equivalent to k_α, if it yields the same ratios of intervortex distances as that of k_α, i.e.,

$$\frac{||k'_\alpha - k'_\beta||}{||k'_2 - k'_1||} = \frac{||k_\alpha - k_\beta||}{||k_2 - k_1||}, \quad 1 \leqslant \alpha < \beta \leqslant N, \tag{20}$$

where $||\cdot||$ denotes the usual Euclidean norm. For example, coordinate transformations such as rotation, reflection, translation, and dilation yield equivalent configurations. If k_α and k'_α are equivalent, then they represent the same equilibrium point in the phase plane constituted by the squared ratios of intervortex distances and therefore must be treated as the same. Finally, it may be noted that since (17) is a necessary and sufficient condition for a self-similar vortex configuration, any configuration k'_α equivalent to k_α will also satisfy (17) for some $\lambda'_0 \in \mathbb{R}$.

To avoid above-mentioned redundancies, we assume that (i) at least three of the circulations are nonzero, and (ii) $k_1 = (0, 0)$ and $k_2 = (1, 0)$ by choosing the origin, orienting, and scaling the axes suitably. The second assumption guarantees that any self-similar initial condition obtained is unique up to a reflection along the x axis: these two mirror images will have opposing signs of λ_0. Consequently, there is a one-to-one correspondence between self-similar collapse and expansion initial conditions. We may obtain one from the other either by reversing the signs of the circulations or by finding its mirror image along the x axis.

III. MOTIVATION

This section provides a basic understanding of self-similar vortex configurations using the formulation (17). The simplest nontrivial case of self-similar motion is that of the three-point vortices, which is thus addressed first in Sec. III A. How the configuration matrix can be used to analytically check for the existence of similarity solutions with a given geometrical arrangement of vortices is discussed next in Sec. III B. Finally, in Sec. III C, we use the configuration matrix to define and associate specific numerical errors with vortex configurations to indicate how far a vortex configuration is from self-similar vortex configurations. The numerical errors are then used to study the distribution of self-similar vortex configurations in the space of all four vortex configurations.

A. Self-similar motion of three vortices ($N = 3$)

The similarity solutions of the three-vortex systems are well understood (see, e.g., [23,27]). In particular, deriving the two necessary conditions (3a) and (3b) is sufficient to completely describe the continuum of three-vortex self-similar collapse and expansion configurations associated with any circulation set. Whereas Aref [23] has discussed these two conditions as one of the parametric cases in his complete study of three-vortex motion, Aref [27] derives them from an equivalent definition of similarity solutions.

Here, we revisit the problem of self-similar motion of three-point vortices from the linear algebra perspective (17) to arrive at (3) and to construct collapse initial conditions in a slightly different form from [23,27]. When the number of vortices is three, (17) evaluates to

$$\underbrace{\begin{bmatrix} 0 & 0 & \frac{2A_{123}}{\pi l_{12}^2}\left(\frac{1}{l_{23}^2}-\frac{1}{l_{13}^2}\right) \\ 0 & \frac{2A_{132}}{\pi l_{13}^2}\left(\frac{1}{l_{23}^2}-\frac{1}{l_{12}^2}\right) & 0 \\ \frac{2A_{231}}{\pi l_{23}^2}\left(\frac{1}{l_{13}^2}-\frac{1}{l_{12}^2}\right) & 0 & 0 \end{bmatrix}}_{M} \underbrace{\begin{bmatrix} \Gamma_1 \\ \Gamma_2 \\ \Gamma_3 \end{bmatrix}}_{\Gamma} = \underbrace{\begin{bmatrix} \lambda_0 \\ \lambda_0 \\ \lambda_0 \end{bmatrix}}_{\Lambda}. \tag{21}$$

Rearranging (21), we obtain

$$\frac{\Gamma_3}{l_{12}^2}\left(\frac{1}{l_{23}^2}-\frac{1}{l_{13}^2}\right) = \frac{\lambda_0 \pi}{2A}, \tag{22a}$$

$$\frac{\Gamma_2}{l_{13}^2}\left(\frac{1}{l_{12}^2}-\frac{1}{l_{23}^2}\right) = \frac{\lambda_0 \pi}{2A}, \tag{22b}$$

$$\frac{\Gamma_1}{l_{23}^2}\left(\frac{1}{l_{13}^2}-\frac{1}{l_{12}^2}\right) = \frac{\lambda_0 \pi}{2A}, \tag{22c}$$

where $A = A_{123} = -A_{132} = A_{231}$ denotes the signed area of the vortex triangle, which is assumed to be nonzero. Since we do not want the system to reduce to a trivial two-vortex system, the three circulations are also assumed to be nonzero. Substituting $\lambda_0 = 0$ in (22) yields $l_{12} = l_{13} = l_{23}$. Hence, irrespective of the values of the three circulations, the equilateral triangle configuration is the only noncollinear rigid-vortex configuration of three vortices.

We shall focus our attention on the three-vortex self-similar collapse and expansion configurations ($\lambda_0 \neq 0$) in the remainder of this section. Simplifying the equation obtained by adding Γ_1 times (22b), Γ_2 times (22c), and $-(\Gamma_1 + \Gamma_2)$ times (22a), we get

$$\Gamma_3 = -\frac{\Gamma_1\Gamma_2}{\Gamma_1 + \Gamma_2} \quad \text{or} \quad \Gamma_1\Gamma_2 + \Gamma_1\Gamma_3 + \Gamma_2\Gamma_3 = 0, \tag{23}$$

which is nothing but the known necessary condition (3a). Without loss of generality, let us assume the initial vortex coordinates to be $k_1 = (0, 0)$, $k_2 = (1, 0)$, and $k_3 = (x, y)$. Subtracting (22c) from (22b) and simplifying the resulting equation yields the relation

$$\omega = f(x, y) := \frac{1 - x^2 - y^2}{(x - 1)^2 + y^2 - 1}, \quad \text{where } \omega = \Gamma_2/\Gamma_1 \tag{24}$$

which must be satisfied by any self-similar collapse and expansion initial condition. Since all three circulations are assumed to be finite nonzero constants, the initial location of the third vortex (x, y) for which (i) $f(x, y) = 0$, (ii) $1/f(x, y) = 0$, and (iii) $f(x, y) = -1$ cannot result in self-similar collapse or expansion. Thus, apart from a zero measure set consisting of two unit circles centered at (0,0) and (1,0), and the lines $x = \frac{1}{2}$ and $y = 0$, the third vortex can be placed anywhere on the plane to obtain a self-similar collapse and expansion configuration for appropriate values of the three circulations satisfying (23) and (24). However, we shall see in Sec. III B that for larger vortex systems, almost none of the configurations tend to be self-similar.

On the other hand, if we were to consider a fixed set of circulations, satisfying (23), and look for all points (x, y), which yield self-similar collapse or expansion configuration, (24) then represents an equation of a level curve in the two-dimensional plane. Note that (24) can be rewritten as

$$\left(x - \frac{\omega}{1 + \omega}\right)^2 + y^2 = \frac{1 + \omega + \omega^2}{(1 + \omega)^2}, \tag{25}$$

which represents a circle with radius $R(\omega) = (1 + \omega + \omega^2)^{1/2}/|1 + \omega|$ and center on the x axis at $x_0(\omega) = \omega/(1 + \omega)$. The circle described by Aref [23,27] has a different center and radius due to the difference in the coordinate representations of the configurations arising from the choice of k_1 and k_2 [see, e.g., Fig. 1(b)].

The circular contours of f for various values of ω are shown in Fig. 3(a). Recall that each circle represents the locus of all possible locations of the third vortex in self-similar collapse or expansion configurations associated with a specific choice of circulations. The vortex positions k_1 and k_2 are marked as green and blue filled circles, respectively. The dashed vertical line $x = \frac{1}{2}$ represents the circle of infinite radius ($\omega = -1$) and corresponds to the limit case of infinite Γ_3 value [see (23)]. Since inverting ω is equivalent to simply interchanging the indices of first and second vortices, we have $R(\omega) = R(1/\omega)$, and the circles are mirror images along the line $x = \frac{1}{2}$. Two representative contours looking at the particular cases of $\omega = -\frac{1}{2}$ and $\omega = -2$ are shown in Fig. 3(b). Six vortex triangle configurations associated with these two circles are highlighted via shading to illustrate the apparent symmetry of self-similar vortex configurations along the $y = 0$ and $x = \frac{1}{2}$ lines.

Each circle intersects the x axis twice at $x_0(\omega) \pm R(\omega)$, which corresponds to two collinear configurations. It can be verified that they are collinear rigid-vortex configurations satisfying (9). Moreover, every contour intersects the $x = \frac{1}{2}$ line twice at $(\frac{1}{2}, \pm\sqrt{3}/2)$ (marked by red filled circles), which corresponds to the equilateral triangle rigid-vortex configuration mentioned before. Hence, for a fixed set of circulations satisfying the necessary condition (23), the three-vortex self-similar collapse and expansion configurations exist as a continuum with a few sandwiched rigid-vortex

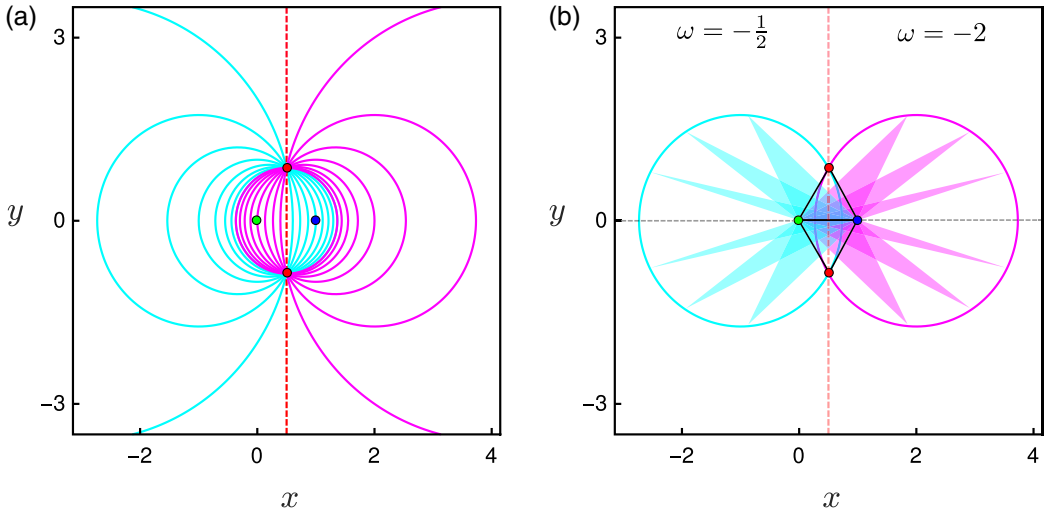

FIG. 3. (a) Contours of $f(x, y)$ for $\omega \in [-1.2, 1.2]$ (cyan) and $1/\omega \in [-1.2, 1.2]$ (magenta) [see Eq. (24)]; (b) six vortex triangles associated with each of the contours $f(x, y) = -\frac{1}{2}$ and $f(x, y) = -2$ (highlighted via shading) show the reflective symmetry of the vortex configurations in the family along the x axis and $x = \frac{1}{2}$ line (red dashed line). The green and blue filled circles denote the location of the first two vortices assumed to be at $k_1 = (0, 0)$ and $k_2 = (1, 0)$, respectively.

configurations. To have a better understanding, let us look at how the Hamiltonian $\mathcal{H}$ and λ_0 vary along a typical continuum of self-similar vortex configurations.

For a given value of ω the associated circular contour can be parametrized as

$$x(\theta) = x_0 + R\cos\theta, \quad y(\theta) = R\sin\theta, \quad 0 \leqslant \theta < 2\pi. \tag{26}$$

Using the above parametrization, we may express both λ_0 and the Hamiltonian $\mathcal{H}$ as a function of θ. For illustration purposes, we examine a specific family of self-similar vortex configurations associated with $\omega = -2$, for which one possible set of circulations is $\Gamma_1 = 1$, $\Gamma_2 = -2 = \Gamma_3$. For this choice of circulations, the variations of λ_0 and $\mathcal{H}$ with parameter θ are shown in Fig. 4. Clearly, $\theta = 0,\ \pi$, implies $y(\theta) = 0$, corresponds to the third vortex lying on the real line. Since, by construction, the first two vortices are always assumed to be at (0,0) and (1,0) in the initial conditions, the three vortices are collinear exactly at $\theta = 0,\ \pi$. Because collinear configurations can only be rigid-vortex configurations, we have $\lambda_0|_{\theta=0} = 0 = \lambda_0|_{\theta=\pi}$. Furthermore, it has already been established that the equilateral triangle and collinear configurations are the only rigid-vortex configurations, hence, other zeros of λ_0 must correspond to equilateral triangle configurations. Since the vortex configurations when the third vortex is at (x, y) and $(x, -y)$ are equivalent, the two graphs are symmetric with respect to $\theta = \pi$, albeit with a sign reversal in the case of λ_0. Hence, we only need to inspect the graphs for $\theta \in [0, \pi]$. The parameter λ_0 oscillates between positive (self-similar expansion configurations) and negative values (self-similar collapse configurations) in a continuous fashion with zeros corresponding to the rigid-vortex configurations, which are marked in the figure with small circles. Furthermore, along the continuum of configurations, the rate of change of $\mathcal{H}$ is nothing but a constant multiple of λ_0, which has the form (see Appendix B for the derivation)

$$\frac{d\mathcal{H}}{d\theta} = \frac{\Gamma_3}{2}\lambda_0. \tag{27}$$

Thus, the rigid-vortex configurations present in the family of self-similar vortex configurations correspond to the critical points of the Hamiltonian function.

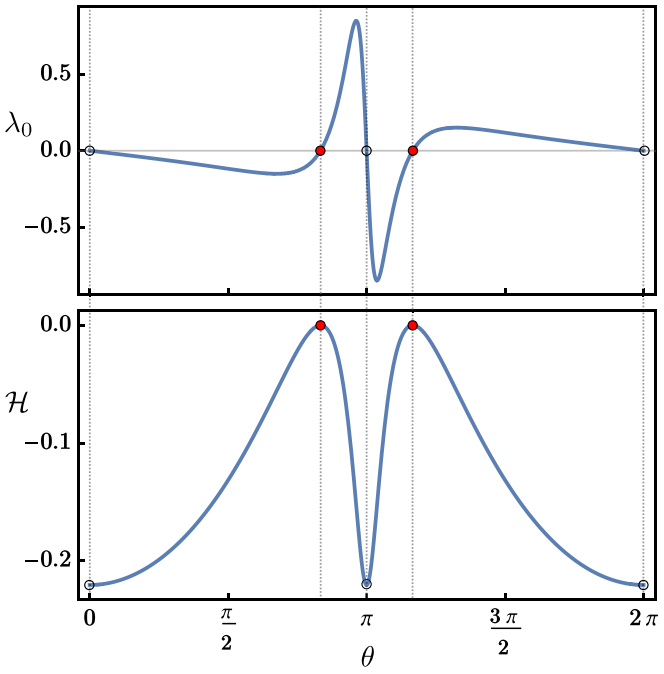

FIG. 4. The variation of λ_0 and Hamiltonian $\mathcal{H}$ with polar coordinate θ for $\omega = \Gamma_2/\Gamma_1 = -2$. The red filled circles correspond to the equilateral triangle configurations [cf. Fig. 3(b)] and unfilled circles to the collinear configurations.

Figure 4 indicates that it is more natural to consider the whole continuum of self-similar vortex configurations associated with a circulation set instead of restricting it to only the collapse or expansion configurations. For instance, looking for the self-similar collapse configurations alone may yield several isolated pieces of continua of vortex configurations which may all be described by a single family of self-similar vortex configurations. Since the configurations in the continuum have a continuous dependence on λ_0 just as the Hamiltonian, it can be potentially used to distinguish between sufficiently close self-similar vortex configurations of the family, replacing the Hamiltonian used in [34,36]. Moreover, the parameter λ_0 is a natural candidate to be used here, as it is directly involved in the formulation (17), unlike the Hamiltonian function.

B. Existence of similarity solutions with a given shape

We can use formulation (17) to check whether it is possible to associate circulations to point vortices arranged in a particular geometrical shape so that the resulting vortex system moves in a self-similar fashion. This is done by first giving a coordinate representation for the vortex configuration with the given shape and then checking whether or not the linear system (17) has a nontrivial solution Γ. If there exists a Γ satisfying (17) for some $\lambda_0 \neq 0$, then one can always scale the circulations by $-1/\lambda_0$ to obtain an equivalent linear system with $\lambda_0 = -1$. Hence, the two right-hand sides $\Lambda_1 = [0, 0, \ldots, 0]^\mathsf{T}$ and $\Lambda_2 = [-1, -1, \ldots, -1]^\mathsf{T}$ in (17) represent the mutually exhaustive cases $\lambda_0 = 0$ (rigid-vortex configuration) and $\lambda_0 \neq 0$ (self-similar collapse and expansion configuration), respectively. Note that any Γ that satisfies $M\Gamma = \Lambda_1$ belongs to the null space of M. Hence, having at least one nonzero circulation set Γ translates to the nullity, the dimension of the null space, being at least one. On the other hand, the linear system $M\Gamma = \Lambda_2$ has at least one solution Γ if and only if Λ_2 is in the column space of the matrix M. Consequently,

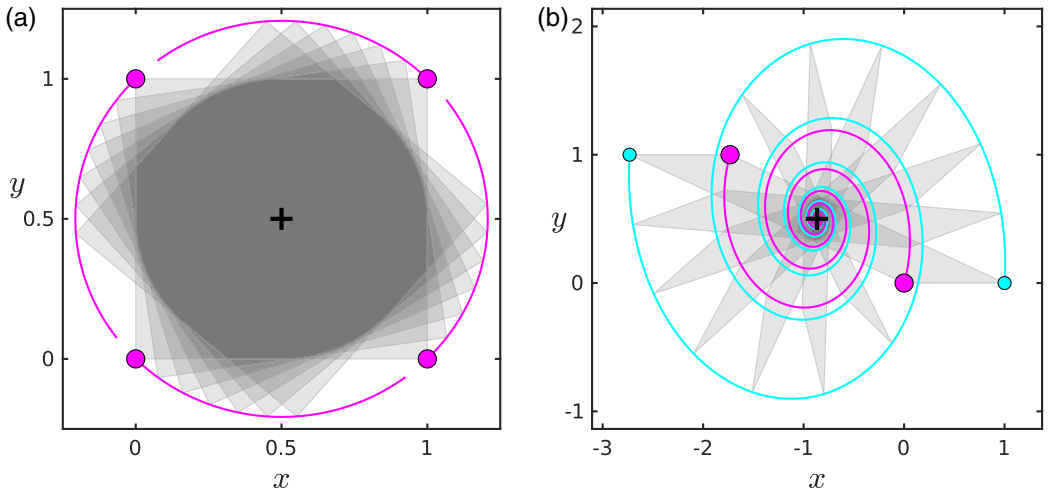

FIG. 5. Self-similar vortex motion associated with the (a) square shape and (b) parallelogram shape given by (28) and (30), respectively. The filled circles denote the initial location of vortices, and the center of vorticity is marked by a plus symbol. Shaded configurations highlight the overall shape and size of the vortex configurations at different instances of motion.

the rank of both M and the augmented matrix $[M|\Lambda_2]$ should be the same. The solutions of both linear systems can be found by row reduction.

To explain the points mentioned above through examples, let us first consider a vortex arrangement in the form of a square shape. Without loss of generality, we may consider the vortex coordinates as

$$k_1 = (0, 0), \quad k_2 = (1, 0), \quad k_3 = (0, 1), \quad k_4 = (1, 1). \tag{28}$$

For these coordinates, the configuration matrix M reads as

$$M = \frac{1}{2\pi}\begin{bmatrix} 0 & 0 & -1 & 1 \\ 0 & 1 & 0 & -1 \\ 0 & 0 & 0 & 0 \\ 0 & 0 & 0 & 0 \\ -1 & 0 & 1 & 0 \\ 1 & -1 & 0 & 0 \end{bmatrix}. \tag{29}$$

Since zero rows are present in the matrix M, the associated λ_0 can only be zero. Hence, there are no self-similar collapses or expansions of point vortices with the square shape. From row reduced echelon form, it can be shown that the null space of M is spanned by $[1, 1, 1, 1]^{\mathsf{T}}$, and that the nullity of M is one. Therefore, the only self-similar motion with a square shape is the rigid-vortex motion by four vortices of equal circulations, as shown in Fig. 5(a). In Fig. 5(a), the trajectories of four identical point vortices initially located at (28) (marked by small filled circles) are shown. The shape of the vortex configuration at different instances of motion is highlighted via shading. It can be seen that vortices move in circular orbits around the center of vorticity (marked by a plus symbol) and retain both the size and shape of the initial configuration (28) throughout the motion. The trajectories are numerically obtained by integrating the system (6) using the fourth-order Runge-Kutta method.

Next, we consider a particular parallelogram shape given by

$$k_1 = (0, 0), \; k_2 = (1, 0), \; k_3 = (-1 - \sqrt{3}, 1), \; k_4 = (-\sqrt{3}, 1), \tag{30}$$

which yields the following configuration matrix M:

$$M = \frac{52}{\pi}\begin{bmatrix} 0 & 0 & 6-5\sqrt{3} & 7-8\sqrt{3} \\ 0 & \sqrt{3}+4 & 0 & 6\sqrt{3}-15 \\ 0 & 2(\sqrt{3}+4) & 2(\sqrt{3}+4) & 0 \\ 4\sqrt{3}-10 & 0 & 0 & 4\sqrt{3}-10 \\ 6\sqrt{3}-15 & 0 & \sqrt{3}+4 & 0 \\ 7-8\sqrt{3} & 6-5\sqrt{3} & 0 & 0 \end{bmatrix}. \tag{31}$$

Note that the rank of M is 4, and the nullity is zero from the rank-nullity theorem. Hence, there are no rigid-vortex configurations with this particular shape. On the other hand, solving the linear system (17) with M being given by (31) and $\lambda_0 = -1$ by row reduction yields a solution

$$\Gamma = \pi\,[5+2\sqrt{3}, -4+\sqrt{3}, -4+\sqrt{3}, 5+2\sqrt{3}]^{\mathsf{T}}. \tag{32}$$

Hence, a four-vortex self-similar collapse configuration exists with the given parallelogram shape (30), as depicted in Fig. 5(b). Similarly to Fig. 5(a), in Fig. 5(b), small filled circles are used to mark the initial location (30) of the vortices. The size of the filled circles is proportional to the magnitude of the circulations (32), and the magenta (cyan) color is used to denote a vortex with positive (negative) circulation. It can be seen that the vortices approach the center of vorticity (marked as a plus symbol) in logarithmic spirals. The vortex configurations at different instances of time (shown as shaded polygons) also verify that the initial parallelogram shape (30) is preserved throughout the motion.

C. A discussion of $N > 3$ case

For $N > 3$, (17) is an extremely overdetermined system. If the matrix coefficients are assumed to be random, we would expect only the zero solution for $M\Gamma = \Lambda_1$ and no solution for $M\Gamma = \Lambda_2$. To investigate how abundant the vortex configurations that can lead to self-similar motion are, compared to those that can not, we numerically assign a number E with a given configuration as

$$E = \min(E_0, E_1), \tag{33}$$

where

$$E_0 = \sigma_{\min}/\sigma_{\max} \quad \text{and} \quad E_1 = ||M\Gamma_{ls} - \Lambda_2||. \tag{34}$$

Here, $\sigma_{\min}$ and $\sigma_{\max}$ are the smallest and largest singular values of the configuration matrix M, and Γ_{ls} is the least-square solution, which minimizes the norm $||M\Gamma - \Lambda_2||$. Observe that E_0 and E_1 are zero if and only if the linear systems $M\Gamma = \Lambda_1$ and $M\Gamma = \Lambda_2$ have at least one solution, respectively. Therefore, if E is sufficiently close to zero, we could numerically conclude that there is at least one nonzero circulation set for which the given configuration leads to a self-similar motion. As a simple representative case, the variation of logarithmic of E (base 10) is illustrated in Fig. 6 for randomly generated 10^6 quadrilateral configurations as a discrete data plot. There are a total of 10^6 plot points marked by red dots in Fig. 6, and the jth plot point ($j = 1$ to 10^6) corresponds to $\log(E)$ of the jth configuration generated. It is seen that most of the configurations have an associated E value between 1 and 10^{-2}. The number of configurations that has $E < 10^{-6}$ is negligible compared to the number of configurations with $E \geqslant 10^{-6}$. This further implies that, unlike the $N = 3$ case, where almost all triangular configurations have an associated self-similar motion, it is very unlikely that a random configuration of vortices could execute a self-similar motion for $N > 3$.

To better visualize how typical self-similar vortex configurations are distributed among the space of all possible configurations when $N > 3$, we consider a two-dimensional subclass of quadrilaterals

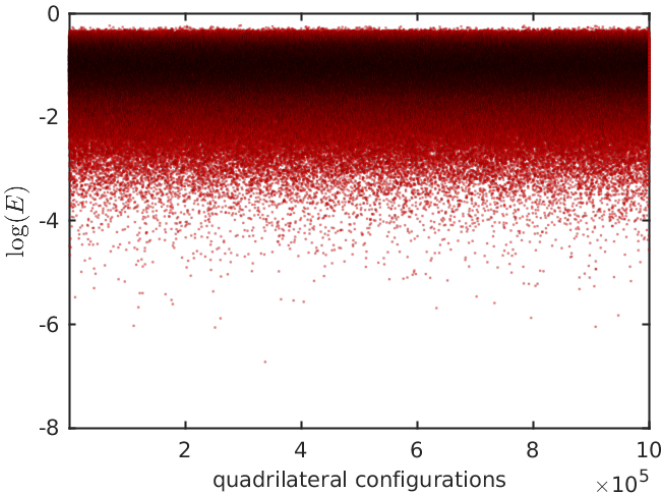

FIG. 6. The discrete data plot of logarithm of E to the base 10 associated with 10^6 randomly generated quadrilateral configurations [see (33)]. Each plot point (marked by red dots) corresponds to the $\log(E)$ value associated with one of the 10^6 configurations.

given by

$$k_1 = (0, 0),\ k_2 = (1, 0),\ k_3 = (x, y),\ k_4 = (x + 1, y), \quad (x, y) \in \mathbb{R}^2. \tag{35}$$

It may be noted that the elements of the above subclass are all parallelogram configurations, each of which is uniquely determined by its location of the third vortex. Associating logarithms of E_0, E_1, and E with third vortex locations of the configurations (35) yield the density plots, Figs. 7(a), 7(b), and 7(c), respectively. Since darker shade indicates a smaller error, points with the darkest shade correspond to rigid-vortex configurations [Fig. 7(a)] and self-similar collapse or expansion configurations [Fig. 7(b)]. Moreover, since E is just the minimum of E_0 and E_1, the density plot of $\log E$, shown in Fig. 7(c), is the same as Figs. 7(a) and 7(b) superimposed. Note that the two previously discussed self-similar configurations [square (28) and parallelogram (30)] are elements of the subclass (35) and are marked with green filled circles in Figs. 7(a) and 7(b), respectively.

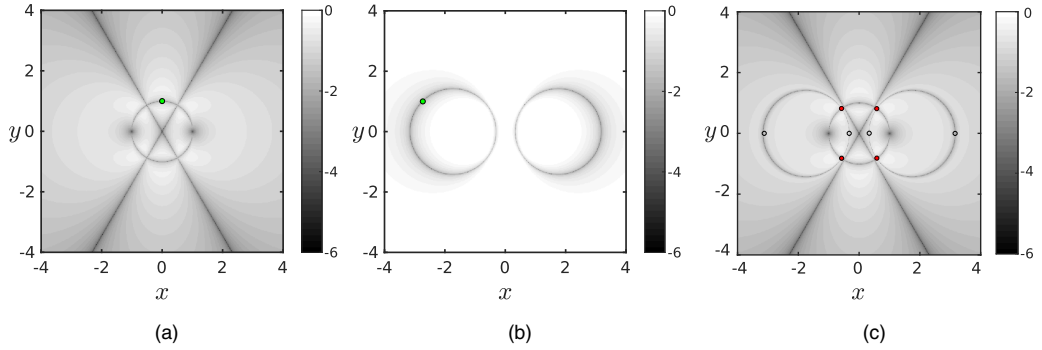

FIG. 7. Density plot of (a) $\log E_0$, (b) $\log E_1$, and (c) $\log E$ in (x, y) plane [see (33) and (34)] associated with the third vortex location in the parallelogram configuration (35). Green filled circle in (a) and (b) denotes the known self-similar configurations (28) and (30), respectively. In (c), the intersection points corresponding to rigid-vortex configurations that are part of the two circular self-similar collapse and expansion continua are marked by small red filled (noncollinear) and unfilled (collinear) circles.

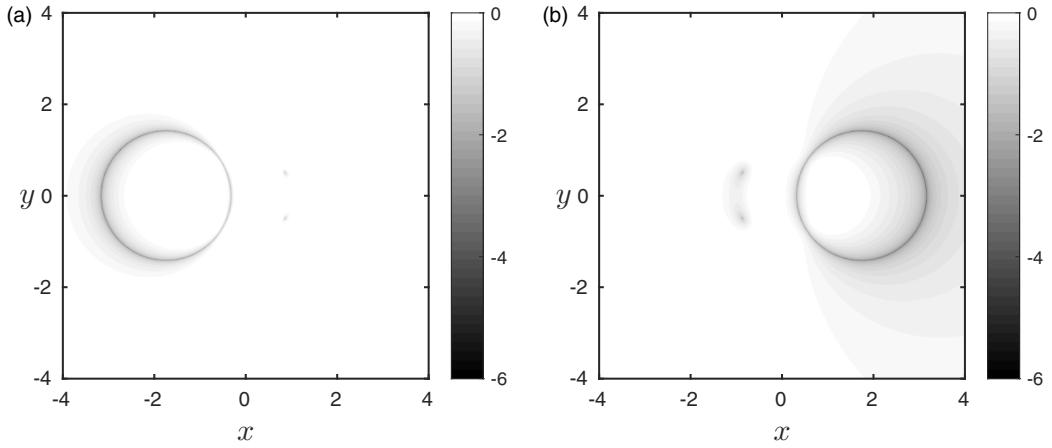

FIG. 8. Density plot of (a) $\log E_2$ and (b) $\log E_3$ in (x, y) plane [see (37)] associated with the third vortex location in the parallelogram configuration (35).

Clearly, only a measure zero set of a continuum of configurations, represented by the continuous black curves in Fig. 7, can lead to a self-similar motion when circulations are chosen appropriately. Let us focus on the two closed self-similar collapse and expansion continua represented by the two circles in Fig. 7(b). We shall now show that all of the self-similar expansion and collapse configurations (35) corresponding to the left and right circles stem from the circulation sets Γ [see (32)] and

$$\Gamma' = \pi\,[11 - 6\sqrt{3}, -4 + \sqrt{3}, -4 + \sqrt{3}, 11 - 6\sqrt{3}]^{\mathsf{T}}, \tag{36}$$

respectively. This is done by as before obtaining density plots (see Fig. 8) of logarithms of

$$E_2 = \frac{\text{std}[M * \Gamma]}{||M||_F} \quad \text{and} \quad E_3 = \frac{\text{std}[M * \Gamma']}{||M||_F}, \tag{37}$$

where std denotes the standard deviation and $||M||_F$ denotes the Frobenius norm, defined as the square root of the sum of the squares of matrix elements. Note that normalization by $||M||_F$ is used to avoid the degenerate case of collinear configurations wherein M becomes the zero matrix. Any self-similar configuration associated with the circulation sets Γ and Γ' will have near-zero values of E_2 and E_3, respectively, because of (17). Consequently, they will be represented by the darkest shaded points in the density plot in Fig. 8. Comparing Figs. 7(b) and 8, it becomes evident that the left circle corresponds to the collapse and expansion family of configurations associated with the circulation set (32) and the right circle, that of the set (36). Note that in the family, the third vortex is parametrized along the circle, as seen in Fig. 7(b), and the parametrization of the rest of the vortices is given by (35). Hence, we see that in the family of collapse and expansion configurations, apart from the first two vortices assumed to be at (0,0) and (1,0), the vortices lie in closed smooth curves, just like in the $N = 3$ case. Furthermore, just like in the $N = 3$ case, the family contains finitely many rigid-vortex configurations that are marked by red filled (noncollinear configuration) and unfilled (collinear configuation) circles in Fig. 7(c).

The above approach may be used to visualize the distribution of self-similar vortex configurations if the configuration space has three or fewer independent parameters. However, we have observed that for $N > 3$, almost all vortex configurations tend to be non-self-similar. Consequently, discretizing the whole space of possible vortex configurations makes it an inefficient method for larger vortex systems. An alternative approach to finding individual self-similar collapse and expansion configurations and their associated families systematically using formulation (17) is discussed in Secs. V and VI, respectively.

IV. NUMERICAL METHOD

A linear algebra formulation solely focusing on the rigid-vortex configurations ($\lambda_0 = 0$) has already been discussed by Newton and Chamoun [37] and Barreiro *et al.* [38]. Thus, this work mainly focuses on $\lambda_0 \neq 0$, which includes self-similar expansion ($\lambda_0 > 0$) and collapse ($\lambda_0 < 0$) configurations. Since the reversal of the signs of either circulations or the y coordinates reverses the sign of λ_0, it suffices to only look for the self-similar collapse configurations while searching for an individual self-similar collapse or expansion configuration. This section explains three strategies to define an error function using the formulation (17). The error functions are defined in such a way that a zero error corresponds to a self-similar vortex configuration. We shall use an easily implementable algorithm based on the random walk procedure explained below to tend the error to a near-zero value systematically.

Step 1: (Initialization) Randomly initialize the vortex coordinates k_α. Since k_1 and k_2 are assumed to be (0,0) and (1,0), we only need to initialize the rest of the $N-2$ vortex coordinates.

Step 2: (Random walk procedure) Randomly select a vortex $\beta \in \{3, 4, \ldots, N\}$ and check whether there is an improved update k'_β on a circle of radius proportional to $\text{err}(k_\alpha)/2^n$ centered around k_β and at randomly generated angles iteratively for $n = 1, 2, \ldots, n_{\max}$, where $n_{\max}$ is the maximum number of iterations. Select a different index and repeat the procedure if no improved update is found even after reaching $n = n_{\max}$.

Step 3: (Termination) If the improved error falls below a certain threshold, terminate the procedure. If not, repeat step 2.

The advantage of this easily implementable random walk procedure is that it is unbiased in its search; hence, it is more likely that we can find all solutions. Moreover, the present method has computationally cheaper iterations, as it does not require the evaluation of derivatives. It may also be used to efficiently generate good initial guesses for various Newton's methods if faster numerical convergence is needed. The three error functions are described in the following subsections.

A. Error 1: Free-vortex circulations

Suppose we do not assume anything on the circulations (i.e., Γ_α's are not known *a priori*), but rather we would like to search for a self-similar vortex configuration satisfying (17) for some $\lambda_0 \neq 0$ and circulations Γ_α. Without loss of generality, we assume $\lambda_0 = -1$, i.e., $\Lambda = [-1, \ldots, -1]^{\mathsf{T}}$. The assumption is based on the fact that Γ_α may be scaled appropriately to obtain $\lambda_0 = -1$ from any solution of (17) with $\lambda_0 \neq 0$. For each vortex configuration given by the coordinates k_α's, we associate an error

$$\text{err1}(k_\alpha) = ||M(k_\alpha) * \Gamma_{ls} - \Lambda||, \tag{38}$$

where

$$\Gamma_{ls} = \min_{X \in \mathbb{R}^{N\times 1}} ||M(k_\alpha) * X - \Lambda||$$

is the least-square solution of the linear system (17), and $M(k_\alpha)$ is the configuration matrix associated with k_α. Clearly, if k_α is a self-similar collapse configuration with $\lambda_0 = -1$ for some choice of circulations $\Gamma \in \mathbb{R}^{N\times 1}$, then $||M(k_\alpha)\Gamma - \Lambda|| = 0$ and by the definition of least-square solution $||M(k_\alpha)\Gamma_{ls} - \Lambda|| = 0$. Therefore, $\text{err1}(k_\alpha) = 0$ if and only if k_α is a self-similar collapse configuration with $\lambda_0 = -1$ and Γ_{ls} being a choice of associated circulations. We have used the backslash operator in MATLAB to find the least-square solutions.

B. Error 2: Fixed-vortex circulations

Suppose we fix the circulations Γ_α beforehand and want to check whether there exist any self-similar vortex configurations for that chosen set of circulations. In other words, we shall search for k_α satisfying (17) for some $\lambda_0 \in \mathbb{R}$, with a fixed Γ vector. With each configuration k_α, we associate

the following error:

$$\text{err2}(k_\alpha) = \text{std}[M(k_\alpha) * \Gamma], \tag{39}$$

where std denotes the standard deviation. Since the sign of λ_0 is known only after the numerical convergence, a solution could be any one of the three types of self-similar initial conditions depending on the sign of λ_0.

C. Error 3: Fixed-vortex circulations and fixed λ_0

Once we find a self-similar collapse initial condition $(k_\alpha, \Gamma_\alpha, \lambda_0)$ using any of the above-defined errors (i.e., err1 or err2), we can use it to search for a nearby self-similar vortex configuration of the same circulation set. This is done by considering the error function

$$\text{err3}(k'_\alpha, \lambda'_0) = ||M(k'_\alpha) * \Gamma - [\lambda'_0, \lambda'_0, \ldots, \lambda'_0]^{\mathsf{T}}||, \tag{40}$$

and minimizing err3 in a close neighborhood of k_α for fixed values of λ'_0 that are sufficiently close to λ_0. Note that $\text{err3}(k'_\alpha, \lambda'_0) = 0$ if and only if k'_α is a self-similar vortex configuration associated with the circulation set Γ and with logarithmic distance decay rate parameter λ'_0.

V. SELF-SIMILAR COLLAPSE AND EXPANSIONS

In this section, we illustrate a few examples of self-similar collapse configurations, which are numerically constructed by minimizing the previously defined error functions err1 and err2 (see Secs. IV A and IV B). The following algorithm is used to find collapse configurations:

1: If circulations are not specified, Set err=err1 Else Set err=err2.
2: Execute the random walk procedure (step 1 to step 3) to minimize err below some tolerance value.

In addition, the self-similar motion of the vortices starting at these vortex positions is verified numerically by integrating (6) using the fourth-order Runge-Kutta method, and confirming that all the intervortex distances simultaneously tend to zero in finite time (see Figs. 9 and 10). All numerical computations are carried out using the MATLAB software.

A. Free-vortex circulations (error 1)

Figure 9 illustrates examples of self-similar vortex collapse configurations for $N = 4$ and 5 [obtained by minimizing the error (38)]. In Fig. 9(a), the initial positions of four-point vortices, marked by the filled circles, are given as

$$k_1 = (0, 0), \quad k_2 = (1, 0), \quad k_3 \approx (1.2295, -0.1278), \quad k_4 \approx (0.4900, -0.2107). \tag{41}$$

The associated circulations are (found post numerical convergence)

$$\Gamma \approx [-2.9852, -2.6854, 1.7625, -0.5061]^{\mathsf{T}}. \tag{42}$$

The size of the filled circles is proportional to the absolute values of the vortex circulations, and the magenta (cyan) color is used to denote vortices with positive (negative) circulations. Note that the collapse time $t_c = -1/\lambda_0 = 1$ since λ_0 was assumed to be -1 while defining the error (38). The vortex trajectories are obtained via numerical integration for $t \in [0, 0.999]$, which shows that vortices do indeed spiral down to the center of vorticity (marked by a + sign) as t approaches t_c. The geometrical shape of the vortex arrangement at different instances of time is shown as shaded polygons, and it can be observed that the shape is preserved during the motion.

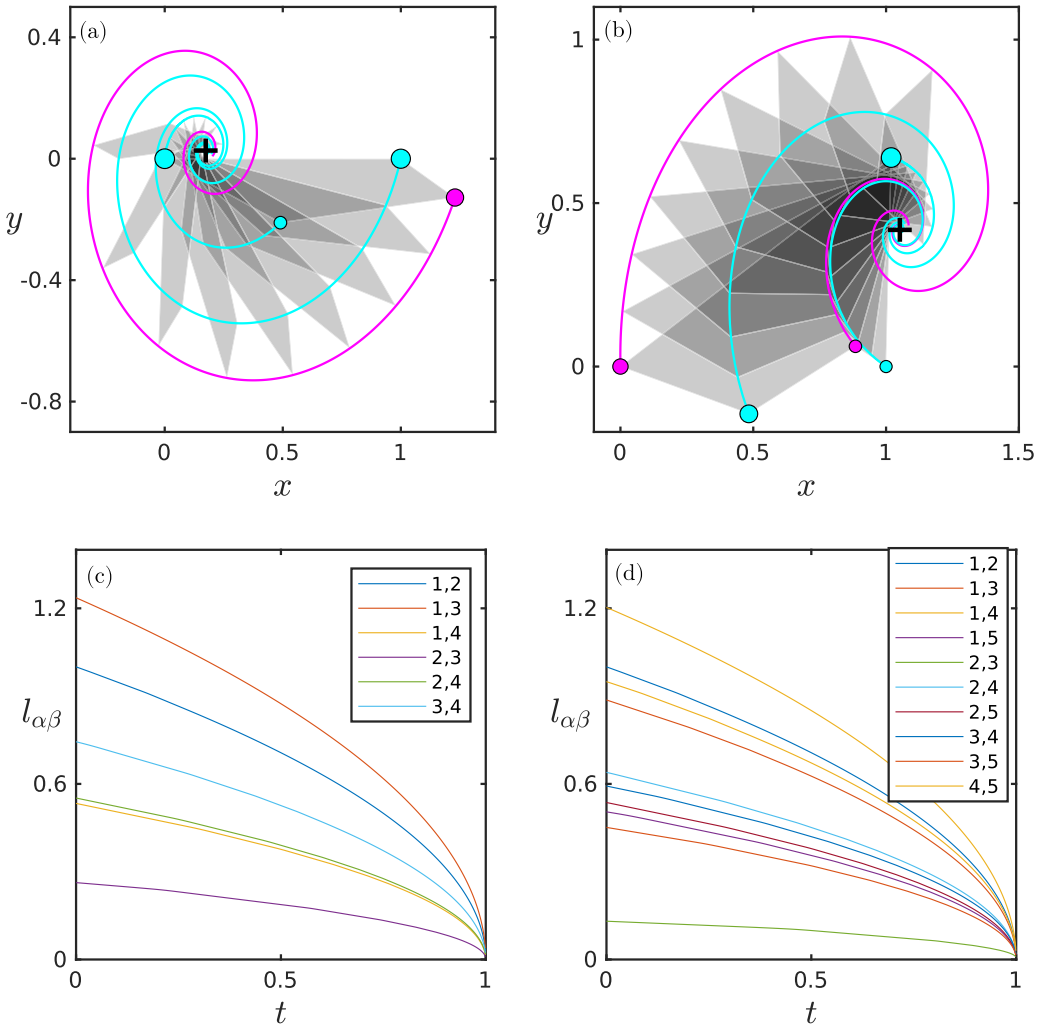

FIG. 9. ($N = 4, 5$) Examples of self-similar vortex collapse configurations (marked by filled circles) by (a) four- and (b) five-point vortices and their respective collapse trajectories for $t \in [0, 0.999]$. The geometrical shapes of the vortex configurations at different instances are shown as shaded polygons. The corresponding intervortex distances vs time graph for (c) $N = 4$ and (d) $N = 5$. The (α, β) indices are used to label the distance functions $l_{\alpha\beta}$.

Similarly, in Fig. 9(b), it can be seen that five-point vortices when placed initially at

$$k_1 = (0, 0),\ k_2{=}(1, 0),\ k_3{\approx}(0.8847, 0.0619),\ k_4 \approx (1.0192, 0.6393),\ k_5 \approx (0.4834, -0.1447) \tag{43}$$

with associated circulations (found post numerical convergence)

$$\Gamma \approx [1.9879, -0.7826, 0.8766, -5.3597, -3.5566]^{\mathsf{T}}$$

executes a self-similar collapse, as evidenced by the constant geometrical shape which is decreasing in size.

The variation of intervortex distances during the self-similar collapse motion [illustrated in Figs. 9(a) and 9(b)] is depicted in Figs. 9(c) and 9(d), respectively. All the 6 distance functions

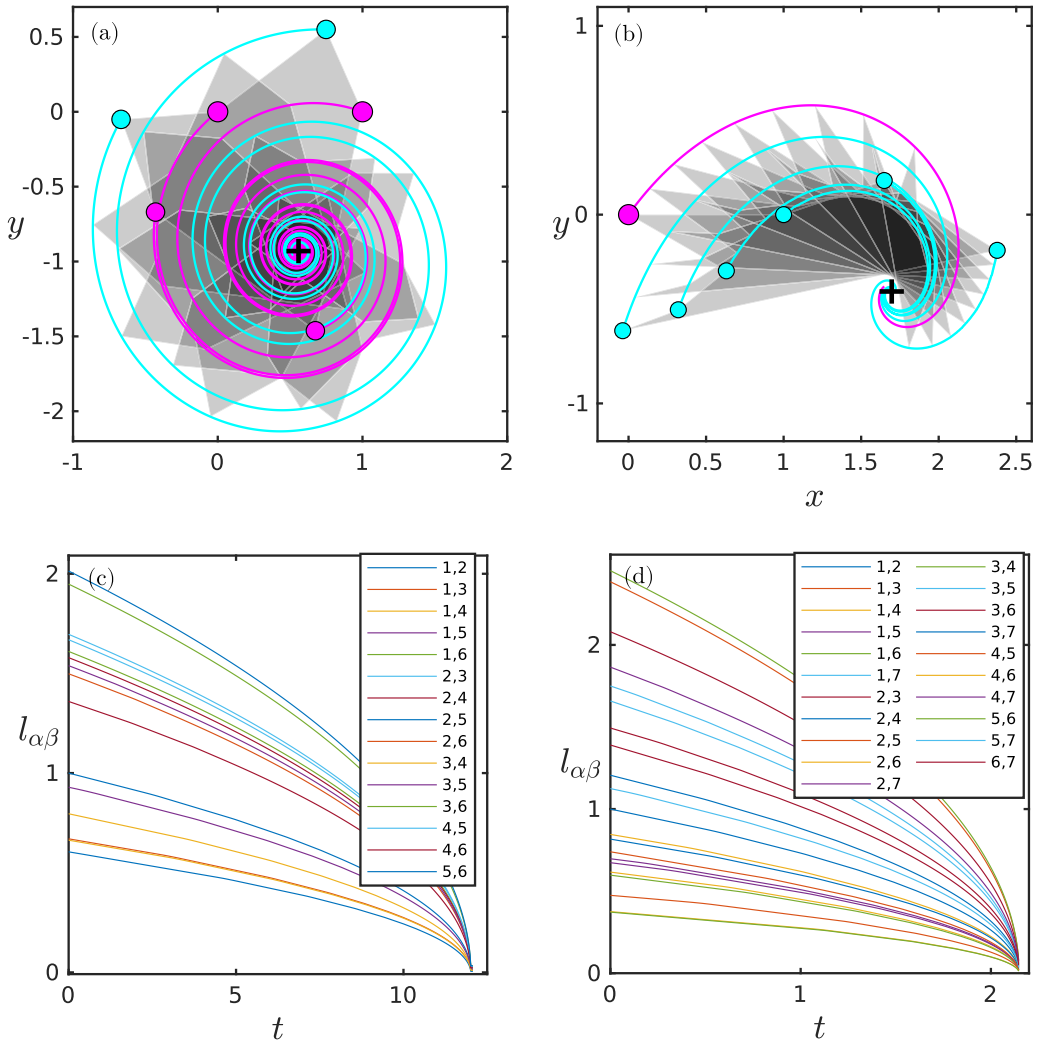

FIG. 10. ($N = 6, 7$) Examples of self-similar vortex collapse configurations (marked by filled circles) by (a) six- and (b) seven-point vortices and their collapse trajectories for $t \in [0, 12.0868]$ and $t \in [0, 2.1479]$, respectively. The geometrical shapes of the vortex configurations at different instances are shown as shaded polygons. The corresponding intervortex distances vs time graph for (c) $N = 6$ and (d) $N = 7$. The (α, β) indices are used to label the distance functions $l_{\alpha\beta}$.

[Fig. 9(c)] in the four-vortex case and 10 in the five-vortex case [Fig. 9(d)] tend to zero as t tends to the unit collision time, indicating the simultaneous vortex collisions at the vorticity center.

B. Fixed-vortex circulations (error 2)

Since the vortex circulations must be known beforehand to define the error (39), we begin by considering two sets of circulations,

$$\Gamma = [\sqrt{2}, \sqrt{2}, -1, 1, -1, 1]^{\mathsf{T}} \tag{44}$$

and

$$\Gamma' = \left[\tfrac{5}{2}, -1, -1, -1, -1, -1, -1\right]^{\mathsf{T}}, \tag{45}$$

which satisfy the necessary condition $\sum \Gamma_\alpha \Gamma_\beta = 0$. Minimizing the error (39) for each of these fixed circulation sets yields self-similar collapse configurations, as shown in Fig. 10. The initial vortex positions in Fig. 10(a) are

$$k_1 = (0, 0), \quad k_2 = (1, 0), \quad k_3 \approx (-0.6683, -0.0507),$$
$$k_4 \approx (-0.4300, -0.6698), \quad k_5 \approx (0.7485, 0.5501), \quad k_6 \approx (0.6744, -1.4623), \tag{46}$$

which are marked by magenta (positive circulation) and cyan (negative circulation) colored filled circles. As before, the vortex trajectories are logarithmic spirals, which maintain the geometrical shape (gray shaded) but shrink in size as the vortices approach the center of vorticity (marked + sign). Similarly, for the second circulation set, vortices initially located at

$$k_1 = (0, 0), \quad k_2 = (1, 0), \quad k_3 \approx (2.3772, -0.1891), \quad k_4 \approx (-0.0377, -0.6149),$$
$$k_5 \approx (0.6306, -0.2977), \quad k_6 \approx (0.3209, -0.5039), \quad k_7 = (1.6487, 0.1807) \tag{47}$$

exhibit a self-similar collapse.

The corresponding variation of intervortex distances with respect to time is illustrated in Figs. 10(c) and 10(d). As expected, the distances all tend to zero in finite time. Since the λ_0 parameter is not prescribed but rather only known post numerical convergence, we have different collision times for the two. For the first set $\lambda_0 \approx -0.0827$ and hence the collision time $t_c \approx 12.0868$ as seen in Fig. 10(c). Similarly, the second one has $\lambda_0 \approx -0.4656$, hence $t_c \approx 2.1479$.

VI. SELF-SIMILAR FAMILY

While investigating the $N = 3, 4$ cases, we observed that for a given circulation set satisfying the necessary condition (3a), the self-similar collapse and expansion configurations exist in the form of $k_\alpha(\theta)$, a continuum of a one-parameter family of configurations [see, e.g., (26)]. Along each family of configurations, λ_0 oscillated between positive and negative values in a continuous fashion with finite zeros, which correspond to rigid-vortex configurations. We assume that $k_\alpha(\theta)$, henceforth referred to as the *self-similar family* of vortex configurations, is a sufficiently smooth function of the parameter θ and propose the following parameter-independent approach to numerically computing it.

1: Find a self-similar collapse configuration $(k_\alpha, \Gamma_\alpha)$ by minimizing err1 or err2.
2: Set $\lambda_0 =$ mean of $[M(k_\alpha) * \Gamma]$.
3: Set $\lambda_0' = \lambda_0 + \delta\lambda_0$, where $|\delta\lambda_0| \ll 1$.
4: Define $\text{err}(k_\alpha') = \text{err3}(k_\alpha', \lambda_0')$.
5: Execute random walk procedure (step 2 to step 3) but using k_α as the initial guess to minimize err below some tolerance.
6: Set k_α^{new} to be the converged solution and k_α^{old} to k_α.
7: **for** $i = 1$ to $n_{\max}$ **do**
8: Define $\delta k_\alpha = h * (k_\alpha^{\text{new}} - k_\alpha^{\text{old}}) / \sqrt{\sum_{\alpha=1}^{N} ||k_\alpha^{\text{new}} - k_\alpha^{\text{old}}||^2}$, where $0 < h \ll 1$.
9: Set $k_\alpha^{\text{guess}} = k_\alpha^{\text{new}} + \delta k_\alpha$
10: Execute random walk procedure (step 2 to step 3) but using k_α^{guess} as the initial guess to minimize err2 below some tolerance.
11: Update k_α^{old} with k_α^{new}.
12: Update k_α^{new} with the converged solution.
13: **end for**

Four examples of self-similar families of vortex configurations (first column) and their associated variation of λ_0 (second column) are shown in Fig. 11. The first two families [Figs. 11(a) and 11(b)

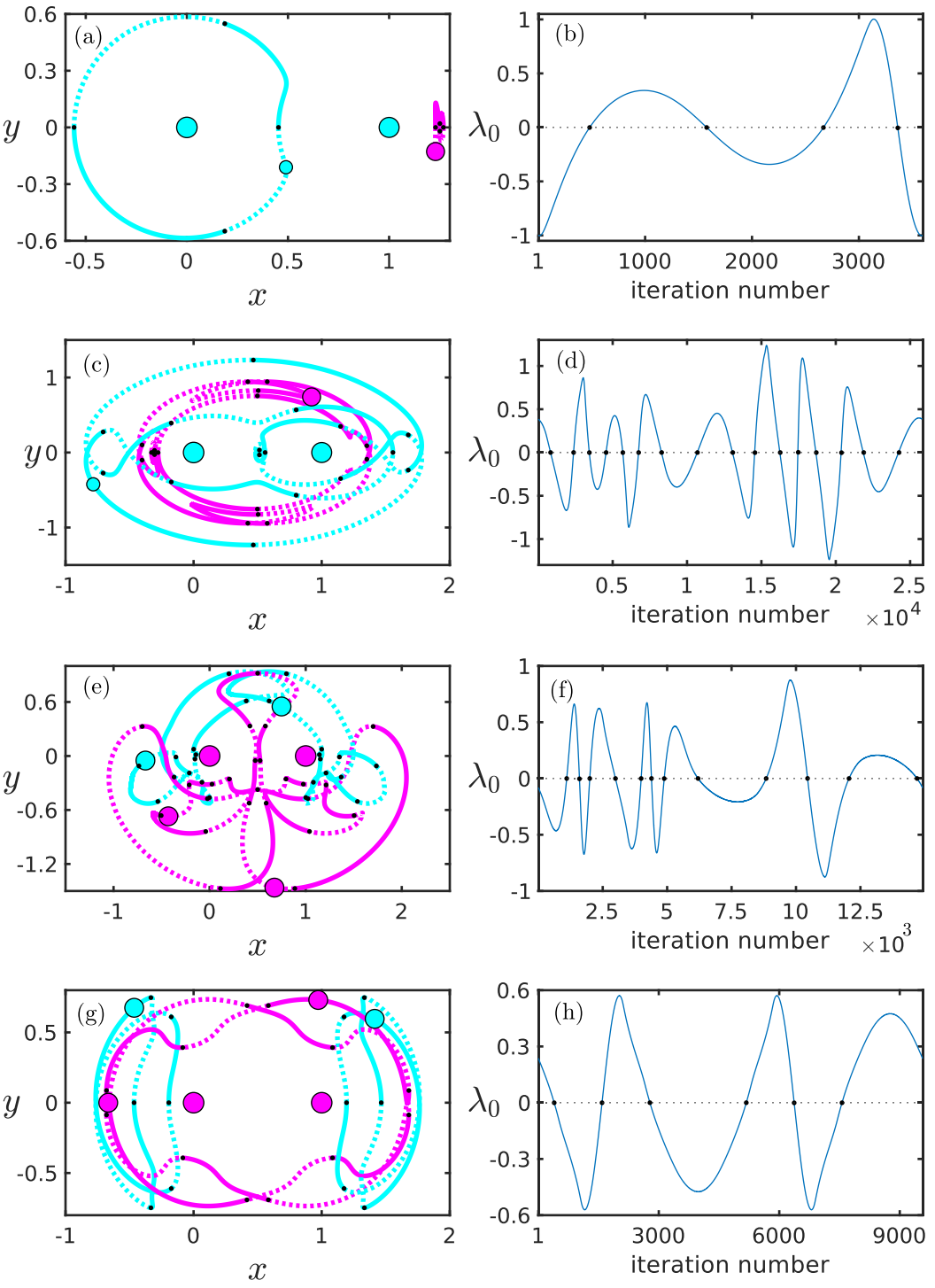

FIG. 11. (a), (c), (e), (g) Examples of self-similar families of vortex configurations (first column) and (b), (d), (f), (h) the associated variation of λ_0 (second column). In (a), (c), (e), and (g), the dotted and solid lines correspond to $\lambda_0 < 0$ and $\lambda_0 > 0$ regimes, respectively, and the filled circles denote the starting configurations used in the algorithm. Black dots denote the rigid-vortex configurations.

TABLE I. Approximate limit configurations in examples 1 and 2.

Index	Circulation	Approximate limit configuration	
		Example 1	Example 2
1	−2	(0,0)	(0,0)
2	−3	(1,0)	(1,0)
3	4	$(1.2186 \times 10^{-3}, -6.1301 \times 10^{-5})$	$(9.4119 \times 10^{-4}, 4.7448 \times 10^{-5})$
4	4	$(-1.2186 \times 10^{-3}, 6.1301 \times 10^{-5})$	$(-9.4119 \times 10^{-4}, -4.7448 \times 10^{-5})$
5	6	(−2.2866, −1.1599)	(−2.2838, 1.1629)

and 11(c) and 11(d)] stem from the circulation set (42), whereas the last two [Figs. 11(e) and 11(f) and 11(g) and 11(h)] originate from (44). The vortex configurations used as the starting points in the algorithm are marked by filled circles in Fig. 11, some of which are the collapse configurations discussed in Sec. V. Solid lines mark the self-similar expansion ($\lambda_0 > 0$) regime, whereas the self-similar collapse ($\lambda_0 < 0$) regime is marked by dotted lines. Black dots spot the rigid-vortex configurations ($\lambda_0 = 0$). It is seen from these examples that there can be multiple disconnected families for a set of circulations. Each self-similar family of configurations comprises the first two vortices assumed to be at (0,0) and (1,0), and the rest of the $N-2$ vortices parametrized along smooth closed planar curves. The two equivalent mirror configurations along the x axis need not be part of the same family, as seen in example 3 [see Figs. 11(c) and 11(d)]. Therefore, the closed structure need not be because of the equivalency of configurations alone. Moreover, whenever the family of configurations has reflective symmetry along the x axis, there appear to be two collinear rigid-vortex configurations present in the family.

Kudela [34] and Gotoda [36] showed that for certain sets of circulations, there exist self-similar families which are not closed, i.e., individual vortex positions of the self-similar family of configurations do not form closed curves. The only discussed example in the literature is a seven-vortex system given by

$$\Gamma_1 = \Gamma_2 = 1, \quad \Gamma_3 = \Gamma_4 = \Gamma_5 = \Gamma_6 = -2, \quad \Gamma_7 = \tfrac{3}{2}. \tag{48}$$

It has been reported that the self-similar family contains a configuration in which the vortices with circulations $\{-2, -2, 1\}$ are located at the same point. The family cannot be extended further once the said configuration is reached. Here, we provide four such examples wherein the self-similar families are not closed; see the first column of Fig. 12. Figures 12(a) and 12(d) are the two pieces of a self-similar family associated with the circulation set

$$\Gamma_1 = -2, \quad \Gamma_2 = -3, \quad \Gamma_3 = \Gamma_4 = 4, \quad \Gamma_5 = 6, \tag{49}$$

with the starting self-similar vortex configuration (marked by filled circles) given by

$$\begin{aligned} &k_1 = (0,0), \quad k_2 = (1,0), \quad k_3 \approx (0.6248, 0.0113), \\ &k_4 \approx (-0.6462, 1.0862), \quad k_5 \approx (-0.7205, -0.0294), \end{aligned} \tag{50}$$

in the decreasing and increasing λ_0 directions, respectively. The approximate values of the two limit configurations (ending configurations) are depicted in Table I. Note that we can only obtain the various orders of approximations of the limit configuration depending on the order of h used in the algorithm and because of the singular nature of the exact limit configuration.

Similarly, Figs. 12(g) and 12(j) are the two pieces of a self-similar family associated with the circulation set

$$\Gamma_1 = -1, \quad \Gamma_2 = \Gamma_3 = 3, \quad \Gamma_4 = -3, \quad \Gamma_5 = \Gamma_6 = 2, \tag{51}$$

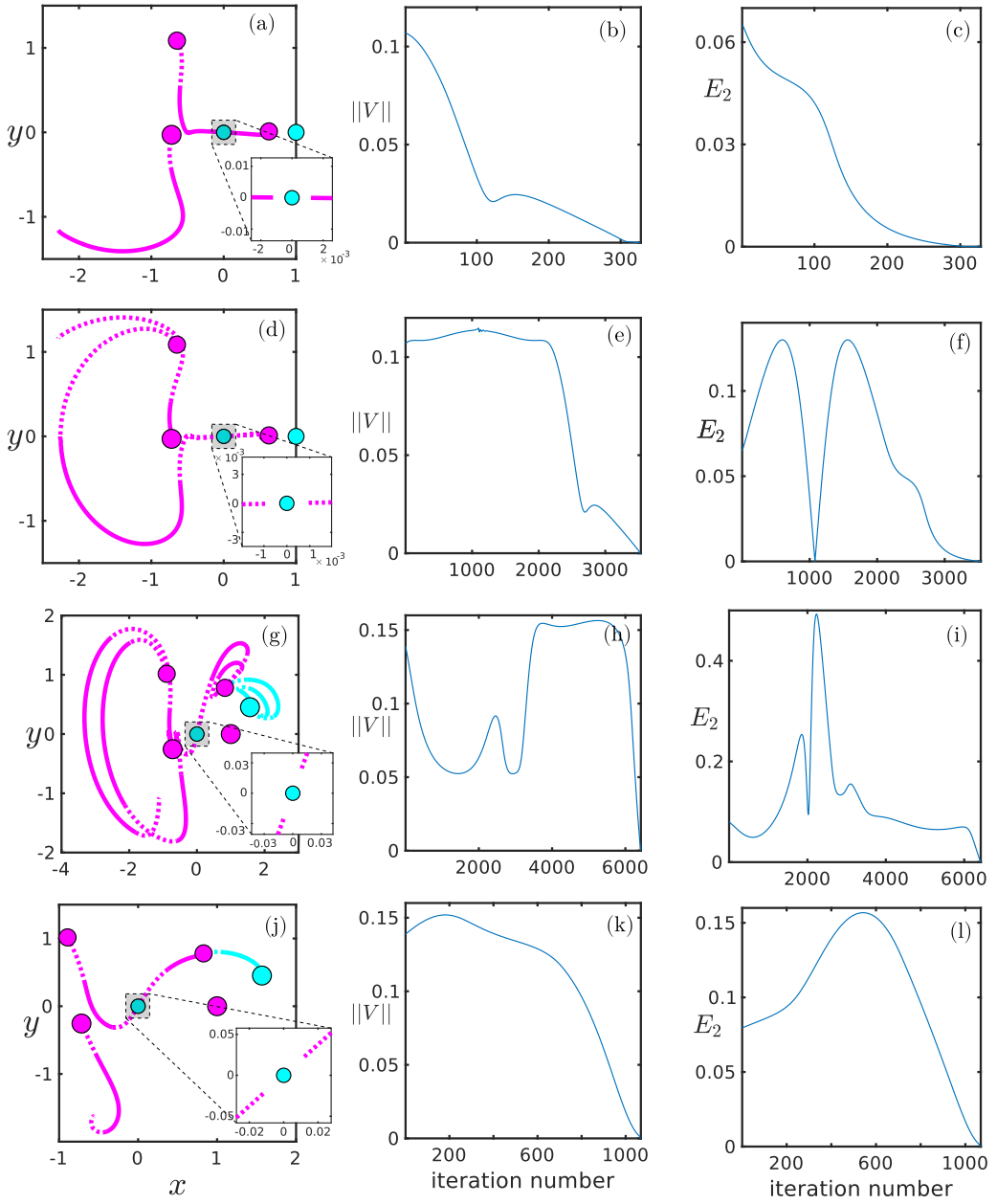

FIG. 12. (a), (d), (g), (j) Self-similar families that are not closed, where insets show the zoomed part of vortex triplet. Variation of norm of velocities $||V||$ of the vortex triplet (b), (e), (h), (k) and $E_2 = \text{err2}$ values of the vortex system with the vortex triplet being considered as a single vortex (c), (f), (i), (l).

with the starting configuration

$$k_1 = (0, 0), \quad k_2 = (1, 0), \quad k_3 \approx (-0.7169, -0.2554),$$
$$k_4 \approx (1.5677, 0.4530), \quad k_5 \approx (0.8288, 0.7800), \quad k_6 \approx (-0.8936, 1.0166), \tag{52}$$

TABLE II. Approximate limit configurations in examples 3 and 4.

Index	Circulation	Approximate limit configuration	
		Example 3	Example 4
1	−1	(0,0)	(0,0)
2	3	(1,0)	(1,0)
3	3	$(-1.1102, -1.0758)$	$(-5.6363 \times 10^{-1}, -1.6198)$
4	−3	$(8.1770 \times 10^{-1}, 7.6858 \times 10^{-1})$	$(7.2154 \times 10^{-1}, 7.5269 \times 10^{-1})$
5	2	$(8.6873 \times 10^{-3}, 2.2768 \times 10^{-2})$	$(1.040 \times 10^{-2}, 2.0758 \times 10^{-2})$
6	2	$(-8.6879 \times 10^{-3}, -2.2767 \times 10^{-2})$	$(-1.1040 \times 10^{-2}, -2.0757 \times 10^{-2})$

in the decreasing and increasing λ_0 directions, respectively. The limit configurations are approximately as given in Table II.

In each of the four examples, as the family tends to the limit configuration, two of the vortex coordinates tend toward the first vortex position at (0,0); see the first column of Fig. 12. On close inspection (see the zoomed figures in the first column), it is observed that the three vortices are asymptotically forming a collinear vortex configuration. Let us focus on these vortex triplets, i.e., on vortices with circulations $\{-2, 4, 4\}$ in the first two examples and $\{-1, 2, 2\}$ in the last two examples, respectively.

Let $\{\alpha, \beta, \gamma\} \subset \{1, 2, \ldots, N\}$ denote the set of indices of three vortices under consideration. To analyze the nature of the limiting collinear configurations we inspect $V = (v_\alpha, v_\beta, v_\gamma)$ of their ordered individual velocities calculated as an independent three-vortex system by considering only the induced velocities from the vortices of the subclass $\{\alpha, \beta, \gamma\}$ [see, e.g., (6)].

We observe that the norm of their velocities

$$||V|| = \sqrt{||v_\alpha||^2 + ||v_\beta||^2 + ||v_\gamma||^2} \tag{53}$$

tends to zero as the configuration of the family tends to the limit configuration (see column 2) in all four examples. Therefore, the collinear configurations asymptotically approached by the vortex triplets are, in fact, fixed equilibrium configurations. Furthermore, if we treat the vortex triplet as a single vortex with the sum of the three individual vortex circulations as its circulation, i.e., in the circulation sets (49) and (51), replacing $\{-2, 4, 4\}$ by 6 and $\{-1, 2, 2\}$ by 3, respectively, yield reduced vortex systems with circulations

$$\{6, -3, 6\} \quad \text{and} \quad \{3, 3, 3, -3\}. \tag{54}$$

Notice that the circulations of the reduced vortex systems (54) satisfy the necessary condition (3a). Assigning the center of vorticity of the vortex triplet as the location of the replaced vortex and keeping the rest of the vortex coordinates the same in the configurations constituting the self-similar family, we obtain a collection of vortex configurations associated with the reduced vortex system (54). The variation of err2 values, denoted by E_2, with iteration number is displayed for each of the four examples (see the third column). It is seen that E_2 tends to zero in all four examples. Therefore, the limit configuration of each self-similar family is such that the associated reduced vortex system is a self-similar configuration. It is worth noting that the first zero of E_2 in Fig. 12(f) is due to the collinearity of the corresponding vortex configuration.

The three vortices that cluster together to form an independent fixed equilibrium configuration have a different length scale than the rest of the vortices. Such clustered vortex configurations are known to exist in the continua of relative and fixed equilibrium configurations [41,42].

VII. RIGID-VORTEX CONFIGURATIONS OF A SELF-SIMILAR FAMILY

Given a self-similar collapse or expansion configuration k_α and the associated circulation set Γ_α of a self-similar family, to find the nearest rigid-vortex configuration of the family, we iteratively change Λ and tend it to the zero vector. To be specific, we use the following algorithm.

1: Set $k_\alpha^{\text{guess}} = k_\alpha$.
2: **for** $i = 1$ to $n_{\max}$ **do**
3: Set $\lambda_0' = \lambda_0 - \dfrac{\lambda_0}{n_{\max}} i$.
4: Define $\text{err}(k_\alpha') = \text{err3}(k_\alpha', \lambda_0')$.
5: Execute random walk procedure (step 2 to step 3) but using k_α^{guess} as the initial guess to minimize err below some tolerance.
6: Update k_α^{guess} with the converged solution.
7: **end for**

In contrast to the algorithm used for finding the self-similar family, the above algorithm involves the parameter λ_0 and can be used to find the rigid-vortex configurations of the family accurately. The algorithm is based on the assumption that λ_0 has a convex graph in the $\lambda_0 < 0$ regime and a concave graph in the $\lambda_0 > 0$ regime, respectively, as seen in the variation of λ_0 with iteration number in Fig. 11. The assumption may be dropped, if the initial configuration k_α is sufficiently close to the rigid-vortex configuration, such that λ_0 varies monotonically along the self-similar family in the direction of the said rigid-vortex configuration. This is achieved by first finding the self-similar family and then initializing k_α with the smallest $|\lambda_0|$ configurations. Although we may find the noncollinear rigid-vortex configurations of the family by minimizing the above-defined error with $\lambda_0' = 0$ (i.e., $i = 1$ to $n_{\max}$), to obtain the collinear ones, we shall instead consider a near-zero value of λ_0' (i.e., $i = 1$ to $n_{\max} - 1$) in order to avoid the degeneracy of the formulation.

A continuum of self-similar collapse configurations tending to a rigid-vortex configuration is constructed from each of the four self-similar collapse examples discussed in Sec. V, by iteratively tending the λ_0 parameter to zero and for each fixed λ_0 minimizing the error (40). Furthermore, the point-vortex equations (6) are numerically integrated with the limit vortex coordinates of the obtained family as initial conditions to verify that they are indeed rigid-vortex configurations characterized by constant intervortex distance functions.

In Fig. 13(a), a continuum of self-similar collapse configurations associated with the circulation set $\Gamma \approx [-2.9852, -2.6854, 1.7625, -0.5061]^{\mathsf{T}}$ is illustrated for $\lambda_0 \in [-1, -0.001]$. The collapse configuration (41) corresponding to $\lambda_0 = -1$ is marked with filled circles, whereas the configuration $k_1 = (0, 0)$, $k_2 = (1, 0)$, $k_3 \approx (1.2290, -0.0001)$, and $k_4 \approx (0.4527, -0.0001)$ corresponding to $\lambda_0 = -0.001$ is marked with filled triangles. The curves all appear to be tending to the x axis as λ_0 approaches zero, indicating a collinear limit. Since -0.001 is close to zero, we would expect the $\lambda_0 = -0.001$ configuration of the family to be a close approximation of the collinear rigid-vortex configuration as verified in Figs. 13(b) and 13(c). In Fig. 13(b), vortex trajectories for $t \in [0, 5.5]$ starting at $\lambda_0 = -0.001$ configuration are shown, and it is a close approximation of uniform circular motion around the center of vorticity (marked by a + sign). Moreover, the intervortex distances also remain approximately constant with time, as seen in Fig. 13(c).

Similarly, in Fig. 13(d), a continuum self-similar collapse configuration associated with the circulation set $\Gamma \approx [1.9879, -0.7826, 0.8766, -5.3597, -3.5566]^{\mathsf{T}}$ is illustrated for $\lambda_0 \in [-1, 0]$. The initial collapse configuration of the family ($\lambda_0 = -1$) given by (43) is marked with filled circles and the ending ($\lambda_0 = 0$) rigid-vortex configuration given by $k_1 = (0, 0)$, $k_2 = (1, 0)$, $k_3 \approx (0.8935, 0.0013)$, $k_4 \approx (0.6730, 0.4249)$, $k_5 \approx (0.7148, -0.3378)$ with filled triangles. Unlike the previous example, we have a noncollinear rigid-vortex configuration, which is verified by looking at the vortex evolution for $t \in [0, 4]$ [see Figs. 13(e) and 13(f)]. The vortex trajectories starting with

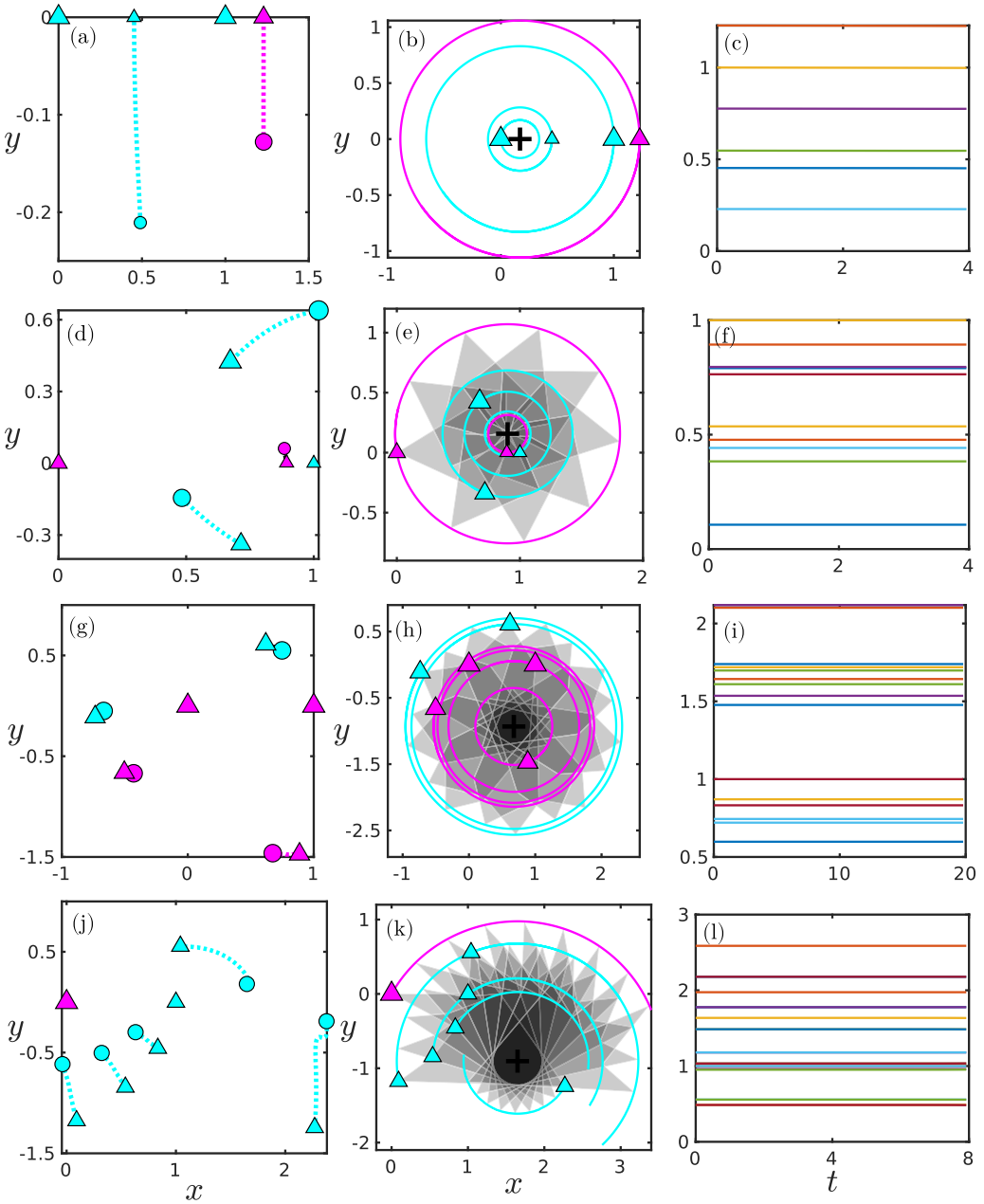

FIG. 13. (a), (d), (g), (j) Self-similar collapse configurations (filled circles) and their nearest rigid-vortex configuration (filled triangles). (b), (e), (h), (k) The rigid-vortex motion (second column), and (c), (f), (i), (l) the associated temporal variation of intervortex distances (third column).

the ($\lambda_0 = 0$) configuration can be seen to be uniform circular motion around the center of vorticity, maintaining constant values of intervortex distances.

A self-similar collapse continuum of the circulation set $[\sqrt{2}, \sqrt{2}, -1, 1, -1, 1]^{\mathsf{T}}$ for $\lambda_0 \in [-0.0827, 0]$ is shown in Fig. 13(g). The initial ($\lambda_0 \approx -0.0827$) configuration (filled circles) has coordinates given by (46) and the end ($\lambda_0 = 0$) configuration (filled triangles) has

coordinates given by $k_1 = (0, 0)$, $k_2 = (1, 0)$, $k_3 \approx (-0.7358, -0.1108)$, $k_4 \approx (-0.5040, -0.6619)$, $k_5 \approx (0.6192, 0.6116)$, $k_6 \approx (0.8871, -1.4724)$. The integrated vortex trajectories of $\lambda = 0$ configurations for $t \in [0, 80]$ are circular around the center of vorticity [see Fig. 13(h)]. The intervortex distance remains constant as expected [see Fig. 13(j)].

Starting with the previously obtained ($\lambda_0 \approx -0.4656$) self-similar collapse configuration (47) of the circulation set $[5/2, -1, -1, -1, -1, -1, -1]^{\mathsf{T}}$, we construct a continuum self-similar collapse configuration for $\lambda_0 \in [-0.4656, 0]$ [see Fig. 13(j)]. The $\lambda_0 = 0$ configuration of the family is given by $k_1 = (0, 0)$, $k_2 = (1, 0)$, $k_3 \approx (2.2688, -1.2440)$, $k_4 \approx (0.0912, -1.1762)$, $k_5 \approx (0.8343, -0.4575)$, $k_6 \approx (0.5377, -0.8431)$, and $k_7 \approx (1.0407, 0.5555)$. The limit configuration is a uniform rotating-type rigid-vortex configuration, as it evolves in circular trajectories around the center of vorticity [see Fig. 13(k)] with constant intervortex distances [see Fig. 13(l)].

VIII. CONCLUSIONS

The similarity solutions of point vortices have been identified as equilibrium points in the phase plane constituted by the intervortex distance ratios. A necessary and sufficient condition for an initial noncollinear vortex configuration to lead to self-similar motion has been found to be the equality of all logarithmic-distance decay rates. The algebraic equations representing this condition are linear in circulations, and of the form $M\Gamma = \Lambda$, where M is a thin matrix (called configuration matrix) that depends solely on the vortex coordinates, Γ is the circulation set as a column matrix, and $\Lambda = [\lambda_0, \ldots, \lambda_0]^{\mathsf{T}}$ is the logarithmic-distance decay rate as a column vector. The sign of the parameter λ_0 determines the type of self-similar motion exhibited: (i) $\lambda_0 > 0$, (ii) $\lambda_0 = 0$, and (iii) $\lambda_0 < 0$ correspond to (i) self-similar expansion, (ii) rigid-vortex motion, and (iii) self-similar collapse, wherein the intervortex distances (i) increase, (ii) remain constant, and (iii) decrease, respectively. Analyzing the distribution of self-similar collapse and expansion configurations for $N = 3$ and 4 showed that they tend to exist as a continuous family of vortex configurations wherein the individual vortex coordinates are parametrized along closed smooth curves. In each family, the associated λ_0 oscillates between positive and negative values, with finitely many zeros corresponding to the finitely many rigid-vortex configurations present in the family. It is more natural to consider the whole continuum of self-similar vortex configurations rather than the pieces constituting only the collapse or expansion configurations. Thus, we have defined a self-similar family of configurations as the continuum of self-similar collapse and expansion configurations associated with a given circulation set, which may also include finitely many rigid-vortex configurations.

Describing the self-similar motion of point vortices through configuration matrices has analytical and numerical advantages over the existing formulations [33,34,36] in the literature. For instance, checking the existence of similarity solutions with any given geometrical arrangement of vortices turns into a routine linear algebra problem of solving $M\Gamma = \Lambda$. Moreover, numerical values can be assigned to vortex configurations through their associated configuration matrix to indicate how close it is to a self-similar vortex configuration, even without knowing the circulations. Three error functions, thus defined using the configuration matrix, have been used appropriately to construct numerical algorithms capable of finding the following: (i) the individual self-similar collapse and expansion configurations with or without the prior knowledge of circulations, (ii) the self-similar family of vortex configurations associated with a circulation set from any given collapse or expansion configuration, and (iii) rigid-vortex configurations associated with a self-similar family.

We have shown from carefully constructed examples that multiple disconnected self-similar families can be associated with a given circulation set. Moreover, we have observed that the closed nature of vortex configurations in self-similar families is not a trivial consequence of symmetry, as some examples do not contain the configurations reflected along the x axis. Furthermore, the circulation sets for which self-similar families of vortex configurations are not closed show an interesting structure. They include a subcollection of circulations satisfying (3a) and the reduced circulation set wherein the subcollection is removed and replaced with the sum of its circulations also satisfies (3a). Inspection of the vortex configurations in some self-similar families showed

that the subcollection of vortices tends to a fixed equilibrium configuration and the reduced vortex system tends to a self-similar vortex configuration as the family approaches the limiting configuration. Thus, it appears that a form of individuality is lost by some of the point vortices at the limit configuration when the self-similar families are not closed. Further studies are required to verify whether or not these observations constitute a necessary and sufficient condition. It is also worth investigating whether λ_0 can have any complex behaviors in a family and whether a fixed equilibrium configuration can be part of a self-similar family of configurations. In the examples we considered, λ_0 had well-behaved convex and concave shaped graphs, and the rigid-vortex configurations of the families were all of the uniformly rotating types.

ACKNOWLEDGMENT

P.S. acknowledges IIT Madras for a New Faculty Seed Grant (Grant No. MAT/1617/671/NFSC/PRIY).

APPENDIX A: NECESSARY CONDITIONS FOR COLLAPSE AND EXPANSION

The two necessary conditions of self-similar vortex collapse are derived using the linear algebra formulation (17).

Lemma 1 (Necessary condition 1). Let $\Gamma_\alpha \in \mathbb{R} \setminus \{0\}$ be the vortex circulations. Any self-similar vortex collapse and expansion initial condition must have $\sum_{\alpha\neq\beta} \Gamma_\alpha \Gamma_\beta = 0$.

Proof. Since point-vortex systems are Hamiltonian systems we have

$$\mathcal{H} = \mathcal{H}|_{t=0}. \tag{A1}$$

Substituting (19) in the above equation yields

$$\sum_{\alpha\neq\beta}^{N} \Gamma_\alpha \Gamma_\beta \log\left(l_{\alpha\beta}^2(0)(1+\lambda_0 t)\right) = \sum_{\alpha\neq\beta}^{N} \Gamma_\alpha \Gamma_\beta \log\left(l_{\alpha\beta}^2(0.)\right) \tag{A2}$$

Subtracting $\mathcal{H}|_{t=0}$ from both sides, we get

$$\log(1+\lambda_0 t) \sum_{\alpha\neq\beta} \Gamma_\alpha \Gamma_\beta = 0, \tag{A3}$$

which is true for any $t \in [0, t_c)$. Therefore, we must have $\sum_{\alpha\neq\beta} \Gamma_\alpha \Gamma_\beta = 0$. ■

Lemma 2 (Necessary condition 2). Let $\Gamma_\alpha \in \mathbb{R} \setminus \{0\}$ be the vortex circulations. If $\{k_\alpha \in \mathbb{R}^2 | \alpha = 1, 2, \ldots, N\}$ is a self-similar collapse or expansion configuration, then $\sum_{\alpha\neq\beta} \Gamma_\alpha \Gamma_\beta l_{\alpha\beta}^2 = 0$, where $l_{\alpha\beta} = ||k_\alpha - k_\beta||$ denotes the intervortex distance.

Proof. From the linear-algebra formulation (16) and the expression (7), for some $\lambda_0 < 0$

$$l_{\alpha\beta}^2 = \frac{2}{\pi\lambda_0} {\sum_{\gamma=1}^{N}}'' \Gamma_\gamma A_{\alpha\beta\gamma} \left(\frac{1}{l_{\beta\gamma}^2} - \frac{1}{l_{\alpha\gamma}^2}\right). \tag{A4}$$

Multiplying both sides by $\Gamma_\alpha \Gamma_\beta$ and summing over all pairs of $(\alpha \neq \beta)$ we get

$$\sum_{\alpha\neq\beta} \Gamma_\alpha \Gamma_\beta l_{\alpha\beta}^2 = \frac{2}{\pi\lambda_0} \sum_{\alpha\neq\beta\neq\gamma} \Gamma_\alpha \Gamma_\beta \Gamma_\gamma A_{\alpha\beta\gamma} \left(\frac{1}{l_{\beta\gamma}^2} - \frac{1}{l_{\alpha\gamma}^2}\right). \tag{A5}$$

Let $S = \sum_{\alpha\neq\beta} \Gamma_\alpha \Gamma_\beta l_{\alpha\beta}^2$. Since the right-hand sum essentially runs over all distinct triplets of indices (α, β, γ), we would expect to get the same result if we interchange the dummy variables α and γ:

$$S = \frac{2}{\pi\lambda_0} \sum_{\alpha\neq\beta\neq\gamma} \Gamma_\alpha \Gamma_\beta \Gamma_\gamma (-A_{\alpha\beta\gamma}) \left(\frac{1}{l_{\alpha\beta}^2} - \frac{1}{l_{\alpha\gamma}^2}\right). \tag{A6}$$

Similarly, if we interchange β and γ,

$$S = \frac{2}{\pi\lambda_0}\sum_{\alpha\neq\beta\neq\gamma}\Gamma_\alpha\Gamma_\beta\Gamma_\gamma\,(-A_{\alpha\beta\gamma})\left(\frac{1}{l_{\beta\gamma}^2}-\frac{1}{l_{\alpha\beta}^2}\right). \tag{A7}$$

Averaging the above three expressions for S we get

$$S = \frac{2}{3\pi\lambda_0}\sum_{\alpha\neq\beta\neq\gamma}\Gamma_\alpha\Gamma_\beta\Gamma_\gamma\,A_{\alpha\beta\gamma}\left(\frac{1}{l_{\beta\gamma}^2}-\frac{1}{l_{\alpha\gamma}^2}-\frac{1}{l_{\alpha\beta}^2}+\frac{1}{l_{\alpha\gamma}^2}-\frac{1}{l_{\beta\gamma}^2}+\frac{1}{l_{\alpha\beta}^2}\right)=0. \tag{A8}$$

Hence, the proof. ■

APPENDIX B: RELATION BETWEEN HAMILTONIAN AND LOGARITHMIC-DISTANCE DECAY RATE

This appendix shows that along the continuum of three-vortex self-similar collapse and expansion configurations associated with a circulation set, the rate of change of Hamiltonian is a scalar multiple of λ_0.

$$\begin{aligned}
\frac{d\mathcal{H}}{d\theta} &= \sum_{\alpha\neq\beta}\frac{\partial\mathcal{H}}{\partial l_{\alpha\beta}^2}\frac{dl_{\alpha\beta}^2}{d\theta} = \frac{-1}{8\pi}\sum_{\alpha\neq\beta}\frac{\Gamma_\alpha\Gamma_\beta}{l_{\alpha\beta}^2}\frac{dl_{\alpha\beta}^2}{d\theta},\\
&= \frac{-\Gamma_3}{4\pi}\left(\frac{\Gamma_1}{l_{13}^2}\frac{dl_{13}^2}{d\theta}+\frac{\Gamma_2}{l_{23}^2}\frac{dl_{23}^2}{d\theta}\right),\\
&= \frac{\Gamma_3 R\,\sin\theta}{2\pi}\left(\frac{\Gamma_1\,\omega/(1+\omega)}{l_{13}^2}+\frac{\Gamma_2(-1/1+\omega)}{l_{23}^2}\right),\\
&= \frac{\Gamma_3 2A}{2\pi(1+\omega)}\left(\frac{\Gamma_2}{l_{13}^2}-\frac{\Gamma_2}{l_{23}^2}\right),\\
&= \frac{-\Gamma_2}{2(1+\omega)}\frac{2A\,\Gamma_3}{\pi}\left(\frac{1}{l_{23}^2}-\frac{1}{l_{13}^2}\right),\\
&= \frac{-\Gamma_2}{2(1+\omega)}\lambda_0 = \frac{\Gamma_3}{2}\,\lambda_0.
\end{aligned}$$

[1] H. Helmholtz, Über integrale der hydrodynamischen gleichungen, welche den wirbelbewegungen entsprechen, J. Reine Angew. Math. **55**, 25 (1858).

[2] O. H. Hald, Convergence of vortex methods for Eulers equations. II, SIAM J. Numer. Anal. **16**, 726 (1979).

[3] J. T. Beale and A. Majda, Vortex methods. II: Higher order accuracy in two and three dimensions, Math. Comput. **39**, 29 (1982).

[4] J. Goodman, T. Y. Hou, and J. Lowengrub, Convergence of the point vortex method for the 2-d Euler equations, Commun. Pure Appl. Math. **43**, 415 (1990).

[5] J.-G. Liu and Z. Xin, Convergence of vortex methods for weak solutions to the 2-d Euler equations with vortex sheet data, Commun. Pure Appl. Math. **48**, 611 (1995).

[6] S. Schochet, The point-vortex method for periodic weak solutions of the 2-d Euler equations, Commun. Pure Appl. Math. **49**, 911 (1996).

[7] C. Marchioro and M. Pulvirenti, Euler evolution for singular initial data and vortex theory, Commun. Math. Phys. **91**, 563 (1983).

[8] B. Turkington, On the evolution of a concentrated vortex in an ideal fluid, Arch. Ration. Mech. Anal. **97**, 75 (1987).
[9] C. Marchioro, Euler evolution for singular initial data and vortex theory: A global solution, Commun. Math. Phys. **116**, 45 (1988).
[10] G. R. Kirchhoff, *Vorlesungen über mathematische physik: Mechanik* (Teubner, 1876), Vol. 1.
[11] H. Aref, Integrable, chaotic, and turbulent vortex motion in two-dimensional flows, Annu. Rev. Fluid Mech. **15**, 345 (1983).
[12] E. A. Novikov and I. B. Sedov, Vortex collapse, Zh. Eksp. Teor. Fiz. **77**, 588 (1979) [Sov. Phys. JETP **50**, 297 (1979)].
[13] R. Benzi, M. Colella, M. Briscolini, and P. Santangelo, A simple point vortex model for two-dimensional decaying turbulence, Phys. Fluids **4**, 1036 (1992).
[14] G. F. Carnevale, J. C. McWilliams, Y. Pomeau, J. B. Weiss, and W. R. Young, Evolution of Vortex Statistics in Two-Dimensional Turbulence, Phys. Rev. Lett. **66**, 2735 (1991).
[15] X. Leoncini, L. Kuznetsov, and G. Zaslavsky, Motion of three vortices near collapse, Phys. Fluids **12**, 1911 (2000).
[16] E. Novikov, Dynamics and statistics of vortex systems, Zh. Eksp. Teor. Fiz. **68**, 1868 (1975) [Sov. Phys. JETP **41**, 937 (1975)].
[17] E. D. Siggia and H. Aref, Point-vortex simulation of the inverse energy cascade in two-dimensional turbulence, Phys. Fluids **24**, 171 (1981).
[18] J. B. Weiss, Punctuated Hamiltonian models of structured turbulence, in *Semi-Analytic Methods for the Navier–Stokes Equations (Crm Proceedings and Lecture Notes)*, edited by K. Coughlin (American Mathematical Society, Providence, RI, 1999), Vol. 20, p. 109.
[19] T. Gotoda and T. Sakajo, Distributional enstrophy dissipation via the collapse of three point vortices, J. Nonlinear Sci. **26**, 1525 (2016).
[20] T. Gotoda and T. Sakajo, Universality of the anomalous enstrophy dissipation at the collapse of three point vortices on Euler-Poincaré models, SIAM J. Appl. Math. **78**, 2105 (2018).
[21] W. Gröbli, *Specielle Probleme über die Bewegung geradliniger paralleler Wirbelfäden* (Druck von Zürcher und Furrer, 1877), Vol. 8.
[22] J. Synge, On the motion of three vortices, Can. J. Math. **1**, 257 (1949).
[23] H. Aref, Motion of three vortices, Phys. Fluids **22**, 393 (1979).
[24] Y. Kimura, Similarity solution of two-dimensional point vortices, J. Phys. Soc. Jpn. **56**, 2024 (1987).
[25] J. Tavantzis and L. Ting, The dynamics of three vortices revisited, Phys. Fluids **31**, 1392 (1988).
[26] Y. Kimura, Parametric motion of complex-time singularity toward real collapse, Phys. D (Amsterdam) **46**, 439 (1990).
[27] H. Aref, Self-similar motion of three point vortices, Phys. Fluids **22**, 057104 (2010).
[28] A. Hernández-Garduño and E. A. Lacomba, Collisions and regularization for the 3-vortex problem, J. Math. Fluid Mech. **9**, 75 (2007).
[29] V. S. Krishnamurthy and M. A. Stremler, Finite-time collapse of three point vortices in the plane, Regul. Chaot. Dyn. **23**, 530 (2018).
[30] T. Sakajo, Non-self-similar, partial, and robust collapse of four point vortices on a sphere, Phys. Rev. E **78**, 016312 (2008).
[31] J. Koiller, S. P. De Carvalho, R. R. Da Silva, and L. C. G. De Oliveira, On Aref's vortex motions with a symmetry center, Physica D (Amsterdam) **16**, 27 (1985).
[32] K. A. O'neil, Relative equilibrium and collapse configurations of four point vortices, Regul. Chaot. Dyn. **12**, 117 (2007).
[33] H. Kudela, Self-similar collapse of n point vortices, J. Nonlinear Sci. **24**, 913 (2014).
[34] H. Kudela, Collapse of n-point vortices in self-similar motion, Fluid Dyn. Res. **46**, 031414 (2014).
[35] K. A. O'Neil, Stationary configurations of point vortices, Trans. Amer. Math. Soc. **302**, 383 (1987).
[36] T. Gotoda, Self-similar motions and related relative equilibria in the N-point vortex System, J. Dyn. Diff. Equ. **33**, 1759 (2021).
[37] P. K. Newton and G. Chamoun, Construction of point vortex equilibria via Brownian ratchets, Proc. R. Soc. London A **463**, 1525 (2007).

[38] A. Barreiro, J. Bronski, and P. K. Newton, Spectral gradient flow and equilibrium configurations of point vortices, Proc. R. Soc. London A **466**, 1687 (2010).
[39] P. K. Newton, *The N-vortex Problem: Analytical Techniques* (Springer, New York, 2013), Vol. 145.
[40] E. A. Coddington and N. Levinson, *Theory of Ordinary Differential Equations* (McGraw-Hill, New York, 1955).
[41] K. A. O'Neil, Clustered equilibria of point vortices, Regul. Chaot. Dyn. **16**, 555 (2011).
[42] K. A. O'Neil, Singular continuation of point vortex relative equilibria on the plane and sphere, Nonlinearity **26**, 777 (2013).